Available online at www.sciencedirect.com
SCIENCE DIRECT®
Journal of Computational Physics 194 (2004) 505–543
JOURNAL OF COMPUTATIONAL PHYSICS
www.elsevier.com/locate/jcp

Eulerian multi-fluid modeling for the numerical simulation of coalescence in polydisperse dense liquid sprays

Frédérique Laurent [a], Marc Massot [a,*,1], Philippe Villedieu [b,c,2]

[a] *MAPLY – UMR 5585, Laboratoire de Mathématiques Appliquées de Lyon, Université Claude Bernard, Lyon 1, 69622 Villeurbanne Cedex, France*
[b] *ONERA, Centre de Toulouse, 2 avenue Edmond-Belin, 31055 Toulouse Cedex 04, France*
[c] *MIP, UMR CNRS 5640, INSA, 135 Avenue de Rangeuil, 31077 Toulouse cedex 04, France*

Received 16 November 2001; received in revised form 11 August 2003; accepted 18 August 2003

Abstract

In this paper, we present a new Eulerian multi-fluid modeling for dense sprays of evaporating liquid droplets which is able to describe droplet coalescence and size polydispersion as well as the associated size-conditioned dynamics. It is an uncommon feature of Eulerian spray models which are required in a number of non-stationary simulations because of the optimization capability of a solver coupling a Eulerian description for both phases. The chosen framework is the one of laminar flows or the one of direct numerical simulations since no turbulence models are included in the present study. The model is based on a rigorous derivation from the kinetic level of description (p.d.f. equation) and can be considered as a major extension of the original sectional method introduced by Tambour et al. We obtain a set of conservation equations for each "fluid": a statistical average of all the droplets in given size intervals associated to a discretization of the size phase space. The coalescence phenomenon appears as quadratic source terms, the coefficients of which, the collisional integrals, can be pre-calculated from a given droplet size discretization and do not depend on space nor time. We validate this Eulerian model by performing several comparisons, for both stationary and non-stationary cases, to a classical Lagrangian model which involves a stochastic algorithm in order to treat the coalescence phenomenon. The chosen configuration is a self-similar 2D axisymmetrical decelerating nozzle with evaporating sprays having various size distributions, ranging from smooth ones up to Dirac delta functions through discontinuous ones. We show that the Eulerian model, if the discretization in the size phase space is fine enough (the problem is then 3D unstationary, 2D in space and 1D in size), is able to reproduce very accurately the non-stationary coupling of evaporation, dynamics and coalescence. Moreover, it can still reproduce the global features of the behavior of the spray with a coarse size discretization, which is a nice feature compared to Lagrangian approaches. The computational efficiency of

* Corresponding author. Tel.: +33-4-72-43-10-08; fax: +33-4-72-44-80-53.
E-mail addresses: laurent@maply.univ-lyon1.fr (F. Laurent), massot@maply.univ-lyon1.fr (M. Massot), Philippe.Villedieu@cert.fr (P. Villedieu).

[1] The present research was done thanks to the support of Université Claude Bernard, Lyon 1, through a BQR grant (Project coordinator: M. Massot), to the support of a CNRS Young Investigator Award (M. Massot, V.A. Volpert) and finally to support of the French Ministry of Research (Direction of the Technology) for the program: "Recherche Aéronautique sur le Supersonique" (Project coordinator: M. Massot).

[2] Tel.: +33-5-62-25-28-63; fax: +33-5-62-25-25-93.

0021-9991/$ - see front matter
doi:10.1016/j.jcp.2003.08.026

both approaches are then compared and the Eulerian model is proved to be a good candidate for more complex and realistic configurations.

1. Introduction

In a lot of industrial combustion applications such as Diesel engines, fuel is stocked in condensed form and burned as a dispersed liquid phase carried by a gaseous flow. Two phase effects as well as the polydisperse character of the droplet distribution in sizes, since the droplets dynamics depend on their inertia and are conditioned by size, can significantly influence flame structures, even in the case of relatively thin sprays [1]. Size distribution effects are also encountered in a crucial way in solid propellant rocket boosters, where the cloud of alumina particles experiences coalescence and become polydisperse in size, thus determining their global dynamical behavior [2]. The coupling of dynamics, conditioned by particle size, with coalescence or aggregation as well as with the eventual evaporation can also be found in the study of fluidized beds [3], planet formation in solar nebulae [4,5]. Consequently, it is important to have reliable models and numerical methods in order to be able to describe precisely the physics of two phase flows where the dispersed phase is constituted of a cloud of particles of various sizes which can evaporate, coalesce or aggregate and finally which have their own inertia and size-conditioned dynamics. Since our main area of interest is the one of combustion, we will work with sprays throughout the paper, keeping in mind the broad application fields related to this study.

Spray models (where a spray is understood as a dispersed phase of liquid droplets, i.e. where the liquid volume fraction is much smaller than one) have a common basis at what can be called "the kinetic level" under the form of a probability density function (p.d.f. or distribution function) satisfying a Boltzmann type equation, the so-called Williams equation [6–8]. The variables characterizing one droplet are the size, the velocity and the temperature, so that the total phase space dimension involved is usually of twice the space dimension plus two. Such a transport equation describes the evolution of the distribution function of the spray due to evaporation, to the drag force of the gaseous phase, to the heating of the droplets by the gas and finally to the droplet–droplet interactions (such as coalescence and fragmentation phenomena) [2,8–13]. The spray transport equation is then coupled to the gas phase equations. The two-way coupling of the phases occurs first in the spray transport equations through the rate of evaporation, drag force and heating rate, which are functions of the gas phase variables and second through exchange terms in the gas phase equations.

There are several strategies in order to solve the liquid phase. A first choice is to approximate the p.d.f. by a sample of discrete numerical parcels of particles of various sizes through a Lagrangian–Monte-Carlo approach [2,9–11,14]. This approach has been widely used and has been shown to be efficient in a number of cases. Its main drawback, that has shown recently to be a major one with the development of new combustion chambers leading to combustion instabilities (lean premixed prevaporized combustor with spray injection), is the coupling of a Eulerian description for the gaseous phase to a Lagrangian description of the dispersed phase, thus offering limited possibilities of vectorization/parallelization and implicitation. Moreover for unsteady computations, a large number of parcels in each cell of the computational domain is generally needed, thus yielding large memory requirement and CPU cost.

This drawback makes the use of a Eulerian formulation for the description of the disperse phase attractive, at least as a complementary tool for Lagrangian solvers, and leads to the use of moments methods since the high dimension of the phase space prevents the use of direct numerical simulation on the p.d.f. equation with deterministic numerical methods like finite volumes. Two classes have been considered before, the first of which is called "population balance" equations [15] for very small particles in the study of

aerosols in chemical engineering; they provide precise and efficient numerical methods in order to follow the size distribution of particles, without inertia, experiencing some aggregation-breakage phenomena (quadrature of moment methods [16,17]). However, the extension of such methods to sprays for which the inertia determines the dynamical behavior of the droplets has not yet received a satisfactory answer. The second type of moment method is the one of moments in the velocity variable without getting into the details of the size distribution or at fixed droplet size: the two-fluid type models used for separated two-phase flows [18–20]. The fact that no information is available on the droplet size distribution is generally too severe an assumption in most applications. One possibility is to use a semi-fluid method based on velocity moment closure of the probability density function at sampled sizes [13]. However, one of the main drawback of most of the existing Eulerian models is the impossibility to treat droplet–droplet interactions because only a finite number of sizes are present in the problem. The use of moments methods leads to the lost of some information but the cost of such methods is usually much lower than the Lagrangian ones for two reasons, the first one is related to the fact that the polydisperse character of the sprays is not described by the model (the spray is mainly considered a mono-dispersed [12]) and the number of unknowns we solve for is very limited; the second one is related to the high level of optimization one can reach when the two phases are both described by a Eulerian model.

A first attempt at deriving a fully Eulerian model for sprays polydisperse in size in laminar configurations with droplets having their own inertia, was developed by Tambour et al. [21]; the idea was to consider the dispersed phase as a set of continuous media: ''fluids'', each ''fluid'' corresponding to a statistical average between two fixed droplet sizes, the section; the spray was then described by a set of conservation equations for each ''fluid''. Greenberg et al. noticed in [21] that such a model has also its origin at the kinetic level trying to make the link with the Williams spray equation [6]. However, they only provided a partial justification, the complete derivation for the conservation of mass and number of droplets, the momentum and energy equations being out of the scope of their paper; besides, the rigorous set of underlying assumptions at the kinetic level was not provided. Finally, their coalescence model did not take into account the relative velocity of colliding particles, thus making the model only suited for very small particles like soots.

A comprehensive derivation of this approach was then provided by Laurent and Massot [8,22,23] for dilute sprays without droplet–droplet interaction in laminar flows, thus yielding a rigorous ''kinetic'' framework, as well as a comparison between Eulerian and Lagrangian modeling. The assumptions underlying the model were validated with experimental measurements on the test case of laminar spray diffusion flames [24]. The idea is to take moments in the velocity variable at each droplet size and space location for a given time: a set of conservation equation is obtained called the semi-kinetic model where the phase space is reduced to the space location and droplet size. The obtained set of conservation equations on the moments in velocity is equivalent to the original p.d.f. equation at the kinetic level under the assumption that there exists a single characteristic velocity at a given space location and droplet size for a given time, around which no dispersion is to be found (the underlying gaseous flow is laminar or the configuration is the one of direct numerical simulations); even if the whole droplet sizes range is covered, the support of the droplet distribution in the phase space is restricted to a 1D sub-manifold of $\mathbb{R}^d$, parametrized by droplet size [8], d being the spatial dimension (it has to be noticed that the same kind of model has been developed and validated in a turbulent framework, where the dispersion around the characteristic velocity at each space location and droplet size is taken to be a variable of the problem instead of being zero [25]). The resulting set of equations which is an extension of the pressureless gas dynamics [26,27] is then discretized in the size variable using a special version of finite volume techniques [28], and we can thus preserve some level of information about the size distribution with a reasonable and adaptive computational cost. If a good level of precision is required about the size distribution, the computational cost is going to be lower but comparable to the Lagrangian one (however the optimization of the solver through the fully Eulerian description of the two phases leads to a substantial gain in CPU

time). The method is still able to capture the behavior of the spray with a coarse discretization in the size phase space [24] and thus a low computational cost, an advantage in comparison with the Lagrangian methods.

In this paper, relying on [8] for the multi-fluid approach analysis and on [29,30] for coalescence phenomena modeling, we derive a Eulerian multi-fluid model for the description of sprays when coalescence is present and thus extend the multi-fluid approach to dense sprays. For the sake of legibility of the paper, this derivation is presented in a simplified framework: we do not take into account convective correction to the vaporization rate and drag force, the unstationary heating of the droplets, as well as the lost of kinetic energy through the coalescence phenomenon; these assumptions are not restrictive as will be explained in the text. This model extension to dense sprays could seem difficult because of the assumption associated with the Eulerian multi-fluid model which is not directly compatible with coalescence. The first step is then to consider Gaussian velocity distributions at a given droplet size with a uniform dispersion. We then derive a semi-kinetic model on the moments of the distribution with a continuous size variable as the limit of zero velocity dispersion. The semi-kinetic model is discretized in fixed size intervals called the sections in order to only treat a finite number of "fluids". We obtain a set of conservation equations on the mass and momentum of the spray for each section with quadratic terms describing the coalescence phenomenon [31], the coefficients of which, the collisional integrals, do not depend on time nor space and can be pre-calculated given a size discretization. We use the numerical method obtained from [32] for the discretization of the conservation equations and the algorithm in order to obtain the pre-calculated collisional integrals is presented.

We want to, firstly, validate this model by with a reference Lagrangian solver which uses an efficient and already validated stochastic algorithm for the description of droplet coalescence [30]. We need a well-defined configuration, both of stationary and unstationary laminar flows where evaporation, coalescence and the dynamics of droplets of various sizes are coupled together. Secondly, we want to evaluate the validity of the assumption underlying the model and the computational efficiency of this new approach as compared to the Lagrangian solver. The configuration has to be complex enough in order to approach some realistic configurations, but simple enough in order to limit the computational cost of the many calculations we want to perform for comparison purposes. The chosen test-case is a decelerating self-similar 2D axisymmetrical nozzle. The deceleration generates a velocity difference between droplets of various sizes and induces coalescence. The temperature of the gas is taken high enough in order to couple the evaporation process to the coalescence one. We consider three types of size distribution functions ranging from smooth ones up to Dirac delta function representing some typical examples of what can be found in combustion applications [24], in booster applications [2] for alumina particles or in chemical engineering. It is worth noticing that such a problem is essentially 2D in space, 1D in the size phase space and unstationary, which makes it equivalent to a 3D unstationary calculation which reduces to a 2D unstationary calculation because of the similarity of the flow. We validate the Eulerian multi-fluid model by showing the good correspondence with the reference solution when the size phase space is finely discretized. It is also shown that the behavior of the spray is correctly captured even if a limited number of "fluids" is used for the Eulerian model corresponding to a coarser discretization in the size phase space. The computational efficiency of the new model is then presented. If a good level of accuracy in the size phase space is required, the cost is lower than the Lagrangian method but not much lower thus showing that, in such a case, the improvement through the use of the Eulerian model is going to be achieved with the optimization of the solver coupling the two Eulerian description. However, the Eulerian model allows an adaptable level of accuracy for the size phase space discretization without having any trouble with the smoothness of the calculated solution (an essential point for combustion applications), a feature which is not present with the Lagrangian solver. We show that a coarse discretization allows to obtain a good qualitative description of the phenomenon; it proves to be very computationally efficient compared to the reference Lagrangian solution and still allows to take into account the polydisperse character of the spray. The level of code optimization that can be

obtained from a global Eulerian description has already been demonstrated in the case of two-fluid models, but the detailed study in the framework of Eulerian multi-fluid models is beyond the scope of the present paper. Finally, the assumption that the velocity dispersion around its mean at a given time, for a given space location and a given droplet size is zero, the Eulerian multi-fluid model relies on, is investigated by considering the results from the Lagrangian solver.

The paper is organized as follows. We present in Section 2 a simplified version of the modeling of the spray at the kinetic level, the purpose of the paper being the clear introduction to a new numerical treatment of sprays. Section 3 is devoted to the exposition of the new Eulerian multi-fluid model. Only the expressions of the intermediate semi-kinetic model and of the final set of conservation equations are provided, the detailed proofs and technical details being presented in Appendices A and B. The numerical methods for the automatic pre-calculation of the collisional integrals are given in Section 4. The validation of the new multi-fluid model is conducted in Section 5, where the nozzle configuration is introduced, the reference Lagrangian solver and the Eulerian multi-fluid one, described and the numerical results presented. Section 6 is devoted to the discussion and conclusion about this new Eulerian multi-fluid model.

2. Modeling of the spray at the kinetic level

For the purpose of the legibility of the paper, we will present the derivation of the Eulerian multi-fluid model for polydisperse evaporating sprays which experience coalescence from a simplified Williams equation at the kinetic level of description [6]. This derivation can easily be extended to a more complex model at the kinetic level as long as a kinetic description of the spray is available and possible; this issue is discussed in the text.

2.1. Williams transport equation

Let us define the distribution function f^α of the spray, where $f^\alpha(t,x,\phi,u,T)\mathrm{d}x\,\mathrm{d}\phi\,\mathrm{d}u\,\mathrm{d}T$ denotes the averaged number of droplets (in a statistical sense), at time t, in a volume of size $\mathrm{d}x$ around x, with a velocity in a $\mathrm{d}u$-neighborhood of u, with a temperature in a $\mathrm{d}T$-neighborhood of T and with a size in a $\mathrm{d}\phi$-neighborhood of ϕ. The droplets are considered to be spherical and characterized by $\phi = aR^\alpha$, where R is the radius of the droplet; ϕ can be the radius ($a = 1$ and $\alpha = 1$; $\phi = R$), the surface, ($a = 4\pi$ and $\alpha = 2$; $\phi = S$) or the volume ($a = \frac{4}{3}\pi$ and $\alpha = 3$; $\phi = v$). We will work with the volume in the following, f^3 will be noted f.

For the sake of simplicity and for the purpose of this paper, we are going to consider that the evaporation process is described by a d^2 law without convective corrections, that the drag force is given by a Stokes law, and finally that the unstationary heating of the droplets does not need to be modeled so that the evaporation law coefficient does not depend on the heating status of the droplet. We refer to [2,33] and [8] for more detailed droplet models for which the derivation can be easily extended.

The evolution of the spray is then described by the Williams transport equation [6]

$$\partial_t f + u \cdot \partial_x f + \partial_v (R_v f) + \partial_u \cdot (Ff) = \Gamma, \tag{2.1}$$

where R_v denoted the d^2 law evaporation rate, F the Stokes drag force due to the velocity difference with the gaseous phase, and Γ the collision operator leading to coalescence. These quantities have the following dependence (t,x,u,v) (except for Γ which is an integral operator depending on f); they depend on the local gas composition, velocity and temperature and this dependence is implicitly written in the (t,x) dependence.

It has to be noticed, firstly, that there is an exact equivalence between the kinetic description and the Lagrangian particulate description of all the droplets (when no droplet interaction nor history terms are to be found) and, secondly, that the refinement of the drag, evaporation and heating models, can not go

beyond a given limit in the context of a kinetic description. The added mass effect in the aerodynamical forces can be described only through the addition of a new variable in the phase space which is the time derivative of the velocity of the particle; in the applications we are considering, it is going to be negligible. Actually, the history terms such as the Basset forces or the inner temperature distribution of a droplet in the effective conductivity model [33] can not be modeled in the context of a kinetic description of the spray, as already discussed in [8]. Moreover, following a droplet history, is not only incompatible with the description in terms of probability density functions, but it would be very difficult to justify the sampling of the spray by a finite number of Dirac delta functions since the phase space in infinite dimensional. Consequently, history terms cannot be accounted for except by augmenting the phase space dimension and by introducing boundary layer variables, a subject beyond the scope of the present study.

As a conclusion, the derivation presented in the following on a simplified model, can be extended to more refined droplet models as long as they do not include history terms. The coalescence model is described in the next section.

2.2. Coalescence operator

The kinetic model for the collision operator leading to coalescence is taken from [29] and we neglect the influence of the impact parameter on the probability of rebound of two collisional partners. We then assume:

[Co1] We only take into account binary collisions (small volume fraction of the liquid phase).
[Co2] The mean collision time is very small compared to the intercollision time.
[Co3] Every collision leads to coalescence of the partners.
[Co4] During coalescence, mass and momentum are conserved.

Thus $\Gamma = Q^-_{\mathrm{coll}} + Q^+_{\mathrm{coll}}$, where Q^-_{coll} and Q^+_{coll}, respectively, correspond to the quadratic integral operators associated with creation and destruction of droplets due to coalescence. These quadratic operators read [2,29]

$$Q^-_{\mathrm{coll}} = -\int_{v^*}\int_{u^*} f(t,x,v,u) f(t,x,v^*,u^*) B(|u-u^*|,v,v^*)\,\mathrm{d}v^*\,\mathrm{d}u^*, \tag{2.2}$$

$$Q^+_{\mathrm{coll}} = \frac{1}{2}\int_{v^*\in[0,v]}\int_{u^*} f(t,x,v^\diamondsuit(v,v^*),u^\diamondsuit(v,v^*,u)) f(t,x,v^*,u^*) B(|u^\diamondsuit-u^*|,v^\diamondsuit,v^*) J\,\mathrm{d}v^*\,\mathrm{d}u^*, \tag{2.3}$$

$$B(|u-u^*|,v,v^*) = \beta(v,v^*)|u-u^*|, \quad \beta(v,v^*) = \pi\left(\left(\frac{3v}{4\pi}\right)^{1/3} + \left(\frac{3v^*}{4\pi}\right)^{1/3}\right)^2, \quad u^\diamondsuit = \frac{vu - v^*u^*}{v-v^*}, \tag{2.4}$$

where $v^\diamondsuit$ and $u^\diamondsuit$ are the pre-collisional parameters, $v^\diamondsuit(v,v^*) = v - v^*$ and J is the Jacobian of the transform $(v,u) \to (v^\diamondsuit,u^\diamondsuit)$, at fixed (v^*,u^*): $J = (v/v^\diamondsuit)^{\mathrm{d}}$, with d the dimension of the velocity phase space.

Remark 2.1. The assumption that all collisions lead to the coalescence of the partners is not realistic, especially if the colliding droplets have comparable sizes [34,35]. In such situations the probability E_{coal}, that coalescence really occurs from the collision of two droplets has to be taken into account; the expression of B then becomes

$$B(|u-u^*|,v,v^*) = E_{\mathrm{coal}}(|u-u^*|,v,v^*)\beta(v,v^*)|u-u^*|.$$

The simplest model, originally obtained for water droplets, was proposed by Brazier-Smith et al. [34] and reads

$$E_{\text{coal}}(|u-u^*|,v,v^*) = \text{Min}\left(1,\frac{\mathscr{F}(v,v^*)}{|u-u^*|^2}\right),$$

where the expression of $\mathscr{F}$ can be found in [34]. Consequently, the expression of E_{coal} is not well-suited for the derivation of our Eulerian multi-fluid model from the kinetic level of description. It is necessary to obtain an approximation of E_{coal} under the form

$$\tilde{E}_{\text{coal}}(|u-u^*|,v,v^*) = \sum_{k=0}^{n} \alpha_k(|u-u^*|)\beta_k(v,v^*), \tag{2.5}$$

with a well-chosen set of functions $(\alpha_k,\beta_k)_{k\in[1,n]}$. A possible choice which leads to easy computations, is to use a polynomial development

$$\tilde{E}_{\text{coal}}(|u-u^*|,v,v^*) = \sum_{k=0}^{n} |u-u^*|^k \beta_k(v,v^*),$$

and to determine the functions $(\beta_k)_{k\in[1,n]}$ by minimizing the the quadratic functional

$$\mathscr{L}(\beta_1,\ldots,\beta_n) = \int_0^{U_{\max}} \sum_{k=0}^{n} \beta_k(v,v^*)W^k - \tilde{E}_{\text{coal}}(W,v,v^*)^2 \mathrm{d}W,$$

where $U_{\max}$ is an estimate of the maximum relative velocity between two droplets; it has to be noticed that the integral in the previous equation can be explicitly calculated, given an expression for $\mathscr{F}$.

Since a statistical description of the spray is needed, and since $\mathscr{F}(v,v^*)$ rapidly becomes bigger than one as the size difference of the coalescence partners increases, a very high degree of precision can be reached with a limited degree of the considered polynomial (2.5).

Nevertheless, in the following, for the sake of simplicity, we will assume

$$E_{\text{coal}}(|u-u^*|,v,v^*) = 1,$$

which is equivalent to assumption [Co3].

3. Eulerian multi-fluid model

In this section, we will recall the formalism and the associated assumptions introduced in [8] in order to derive the Eulerian multi-fluid method and explain how this formalism can be extended in order to treat the coalescence phenomenon between droplets having their own inertia governed by their size. It is worth noticing that we do take into account the mean velocity difference of the droplets in the coalescence process as opposed to the model proposed in [21] which is mainly suited for very small particles such as soots.

The derivation is conducted following two steps. The key idea is to reduce, in a first step, the size of the phase space and to consider only the moments of order zero and one in the velocity variable at a given time, a given position and for a given droplet size. The obtained conservation equations, called the semi-kinetic model for the two fields $n(t,x,v) = \int f \,\mathrm{d}u$ and $\bar{u}(t,x,v) = \int fu\,\mathrm{d}u/n(t,x,v)$, are only in a close form under a precise assumption on the support of the original p.d.f. in the whole phase space: the velocity distribution at a given time, given location and for a given droplet size is a Dirac delta function [8]. These conservation equations are similar to the pressureless gas dynamics [26,27].

However, this assumption is not directly compatible with the coalescence phenomenon. In fact, we obtain the semi-kinetic model in the limit of zero dispersion of a more general problem where dispersion is

allowed. The obtained semi-kinetic model is then equivalent to a projection of the original p.d.f. model onto a lower dimensional configuration.

At this level, we still describe a continuous and unbounded size phase space for the spray. The second step consists in choosing a level of discretization for the droplet size phase space and to average the obtained system of conservation laws over some fixed size intervals, each "fluid" corresponding to the set of droplets in each size interval. It can be interpreted as a finite volume discretization in the size variable, the order of which has been studied in [28] as far as the evaporation is concerned. The coalescence phenomenon, when taken into account, results in quadratic source terms in the Eulerian multi-fluid conservation equations for the mass and momentum of each "fluid". The coefficients involved in these source terms are collisional integrals; they do not depend on t, x or on the droplet size but only on the given droplet size discretization. Consequently, they can be pre-calculated before the resolution of the system of conservation laws is conducted.

3.1. Semi-kinetic model

Out of the assumptions related to the Eulerian multi-fluid model, it was shown in [8] that the velocity dispersion of the spray distribution function at a given time, space location and droplet size has to be zero. It is clear that this assumption is not directly compatible with the coalescence phenomenon, since there is no reason for a droplet created by the coalescence of two droplets of various sizes, which is deduced from momentum conservation, to exactly match the velocity corresponding to its new size. However, since the Eulerian multi-fluid model can be considered as a projection of the original distribution function at the kinetic level onto a 1D sub-manifold, we first relax the assumption of zero dispersion and assume Gaussian velocity dispersion and handle the whole positive real line for the possible sizes so that all the collisions can be described by the model: $(v,u) \in (0,+\infty) \times \mathbb{R}^{\mathrm{d}}$. The semi-kinetic system of conservation laws is then obtained by taking the limit of zero dispersion in the source terms coming from coalescence, uniformly in (t,x,v).

Proposition 3.1. *Let us make the following assumptions on the spray distribution function:*

[H1] *For a given droplet size, at a given point* (t,x), *there is only one characteristic averaged velocity* $\overline{u}(t,x,v)$.

[H2] *The velocity dispersion around the averaged velocity* $\overline{u}(t,x,v)$ *is zero in each direction, whatever the point* (t,x,v).

[H3] *The droplet number density* $n(t,x,v)$ *is exponentially decreasing at infinity as a function of* v *uniformly in* (t,x).

Assumptions [H1] *and* [H2] *define the structure of* f : $f(t,x,v,u) = n(t,x,v)\delta(u - \bar{u}(t,x,v))$ *and the semi-kinetic model is given by two partial differential equations in the variables* $n(t,x,v)$ and $\bar{u}(t,x,v)$:

$$\begin{aligned}\partial_t n + \partial_x \cdot (n\overline{u}) + \partial_v(nR_v) = &- n(v)\int_{v^*\in[0,+\infty)} n(v^*)\beta(v,v^*)I_n^-\,\mathrm{d}v^* \\ &+ \frac{1}{2}\int_{v^*\in[0,v]} n(v^{\diamondsuit}(v,v^*))n(v^*)\beta(v^{\diamondsuit}(v,v^*),v^*)I_n^+\,\mathrm{d}v^*, \end{aligned} \tag{3.1}$$

$$\begin{aligned}\partial_t(n\overline{u}) + \partial_x \cdot (n\overline{u}\otimes\overline{u}) + \partial_v(nR_v\overline{u}) - n\overline{F} = &- n(v)\int_{v^*\in[0,+\infty)} n(v^*)\beta(v,v^*)I_u^-\,\mathrm{d}v^* \\ &+ \frac{1}{2}\int_{v^*\in[0,v]} n(v^{\diamondsuit}(v,v^*))n(v^*)\beta(v^{\diamondsuit}(v,v^*),v^*)I_u^+\,\mathrm{d}v^*, \end{aligned} \tag{3.2}$$

where $\overline{F}$ *is the Stokes's drag force taken at* $u = \overline{u}$, *where* $R_v = R_v(t,x,v)$ *and where the partial collisional integrals* I_n^-, I_n^+, I_u^- *and* I_u^+ *are functions of* (t,x,v,v^*) *and take the following expressions:*

$$I_n^- = |\overline{u}(v) - \overline{u}(v^*)|, \quad I_u^- = \overline{u}(v)|\overline{u}(v) - \overline{u}(v^*)|, \tag{3.3}$$

$$I_n^+ = |\overline{u}(v^*) - \overline{u}(v - v^*)|, \quad vI_u^+ = ((v - v^*)\overline{u}(v - v^*) + v^*\overline{u}(v^*))|\overline{u}(v^*) - \overline{u}(v - v^*)|. \tag{3.4}$$

Eqs. (3.1) *and* (3.2) *express respectively, the conservation of the number density of droplets and their momentum, at a given location* x *and for a given size* v.

The detail of the proof is given in Appendix A and the discussion about the assumption of zero dispersion in the velocity variable will be presented with the numerical simulation on the chosen test case in Section 5.

Remark 3.2. It has to be notice that the coalescence source terms obtained in the system of conservation equations does not conserve the kinetic energy of the droplets as can be easily shown by considering the conservation equation on the second order moment in the velocity variable. It can be assumed that the kinetic energy is dissipated during the coalescence phenomenon, during damped oscillations due to surface tension forces for example, and results in some heating of the droplets. However, for the velocity and the temperature range we are interested in, the change in the temperature of the droplets due to the dissipation of the kinetic energy lost in the coalescence process is totally negligible.

3.2. Eulerian multi-fluid model

The Eulerian multi-fluid model, is based on the reduction of a continuous semi-kinetic equation as a function of size, such as (3.1) and (3.2), to a finite number of degrees of freedom. This reduction is performed by averaging, in fixed size intervals: the sections (the jth section being defined by $v^{(j-1)} \leqslant v < v^{(j)}$), of the semi-kinetic model. As a fundamental assumption, the form of n as a function of the geometry is supposed to be independent of t and x in a given section. Thus the evolution of the mass concentration of droplets in a section $m^{(j)}$ is decoupled from the repartition in terms of sizes $\kappa^{(j)}(v)$ inside the section [21]:

$$n(t,x,v) = m^{(j)}(t,x)\kappa^{(j)}(v), \quad \int_{v^{(j-1)}}^{v^{(j)}} \rho_l v \kappa^{(j)}(v)\,\mathrm{d}v = 1. \tag{3.5}$$

Besides, we make the following assumption on the velocity distribution inside a section:

[H4] In each section, the averaged velocity $\overline{u}(t,x,v)$ does not depend on v, $\overline{u}(t,x,v) = \overline{u}^{(j)}(t,x)$, $v^{(j-1)} \leqslant v < v^{(j)}$.

The sections have fixed sizes, which is a major difference compared to a sampling method; however, they are not independent from each other, they exchange mass and momentum. The choice of the discretization points $v^{(j)}$, $j \in [1,N]$ has been studied in [24]; consequently we choose the $(N+1)$th section to be $[v^{(N)}, +\infty)$ in order to be able to describe the whole size spectrum. The final model is then obtained in the next proposition.

Proposition 3.3. *Assuming* [H1]–[H4], *we obtain the multi-fluid system of* $2(N+1)$ *conservation equations:*

$$\partial_t m^{(j)} + \partial_x \cdot (m^{(j)}\overline{u}^{(j)}) = -(E_1^{(j)} + E_2^{(j)})m^{(j)} + E_1^{(j+1)}m^{(j+1)} + C_{\mathrm{m}}^{(j)}, \tag{3.6}$$

$$\partial_t (m^{(j)}\overline{u}^{(j)}) + \partial_x \cdot (m^{(j)}\overline{u}^{(j)} \otimes \overline{u}^{(j)}) = -(E_1^{(j)} + E_2^{(j)})m^{(j)}\overline{u}^{(j)} + E_1^{(j+1)}m^{(j+1)}\overline{u}^{(j+1)} + m^{(j)}F^{(j)} + C_{\mathrm{mu}}^{(j)}, \tag{3.7}$$

where $E_1^{(j)}$ *and* $E_2^{(j)}$ *are the "classical" pre-calculated evaporation coefficients* [8,21]:

$$E_1^{(j)} = -\rho_l v^{(j)} R_v(t,x,v^{(j)})\kappa^{(j)}(v^{(j)}), \quad E_2^{(j)} = -\int_{v^{(j-1)}}^{v^{(j)}} \rho_l R_v(t,x,v)\kappa^{(j)}(v)\,\mathrm{d}v, \tag{3.8}$$

where $F^{(j)}$ *is the "classical" pre-calculated drag force* [8,21]

$$F^{(j)}(t,x) = \int_{v^{(j-1)}}^{v^{(j)}} \rho_l v \overline{F}(t,x,v)\kappa^{(j)}(v)\,\mathrm{d}v,$$

and where the source terms associated with the coalescence phenomenon, in the mass and momentum equation respectively of the jth section read

$$C_{\mathrm{m}}^{(j)} = -m^{(j)} \sum_{k=1}^{N} m^{(k)} V_{jk} \mathscr{Q}_{jk} + \sum_{i=1}^{I^{(j)}} m^{(o_{ji}^{\diamondsuit})} m^{(o_{ji}^{*})} V_{o_{ji}^{\diamondsuit} o_{ji}^{*}} (\mathscr{Q}_{ji}^{\diamondsuit} + \mathscr{Q}_{ji}^{*}), \tag{3.9}$$

$$C_{\mathrm{mu}}^{(j)} = -m^{(j)} \overline{u}^{(j)} \sum_{k=1}^{N} m^{(k)} V_{jk} \mathscr{Q}_{jk} + \sum_{i=1}^{I^{(j)}} m^{(o_{ji}^{\diamondsuit})} m^{(o_{ji}^{*})} V_{o_{ji}^{\diamondsuit} o_{ji}^{*}} \left(\overline{u}^{(o_{ji}^{\diamondsuit})} \mathscr{Q}_{ji}^{\diamondsuit} + \overline{u}^{(o_{ji}^{*})} \mathscr{Q}_{ji}^{*} \right), \tag{3.10}$$

where $V_{jk} = |\overline{u}^{(j)} - \overline{u}^{(k)}|$ *and where the collision integrals* $\mathscr{Q}_{jk}$, $\mathscr{Q}_{ji}^{\diamondsuit}$ *and* $\mathscr{Q}_{ji}^{*}$ *do not depend on t nor x and read*

$$\mathscr{Q}_{jk} = \int\int_{L_{jk}} \rho_l v \kappa^{(j)}(v)\kappa^{(k)}(v^*)\beta(v,v^*)\,\mathrm{d}v\,\mathrm{d}v^*, \quad \mathscr{Q}_{ji}^{\diamondsuit} = \int\int_{X_{ji}} \rho_l v^{\diamondsuit} \kappa^{(o_{ji}^{\diamondsuit})}(v^{\diamondsuit})\kappa^{(o_{ji}^{*})}(v^*)\beta(v^{\diamondsuit},v^*)\,\mathrm{d}v^*\,\mathrm{d}v^{\diamondsuit}, \tag{3.11}$$

$$\mathscr{Q}_{ji}^{*} = \int\int_{X_{ji}} \rho_l v^* \kappa^{(o_{ji}^{\diamondsuit})}(v^{\diamondsuit})\kappa^{(o_{ji}^{*})}(v^*)\beta(v^{\diamondsuit},v^*)\,\mathrm{d}v^*\,\mathrm{d}v^{\diamondsuit} = \int\int_{X_{ji}^{\mathrm{sym}}} \rho_l v^{\diamondsuit} \kappa^{(o_{ji}^{*})}(v^{\diamondsuit})\kappa^{(o_{ji}^{\diamondsuit})}(v^*)\beta(v^{\diamondsuit},v^*)\,\mathrm{d}v^*\,\mathrm{d}v^{\diamondsuit}. \tag{3.12}$$

$$D_j^{\diamondsuit *} = \bigcup_{k=2}^{N} \bigcup_{l=1}^{k-1} \left(L_{kl} \cap D_j^{\diamondsuit *} \right) \cup \left(L_{lk} \cap D_j^{\diamondsuit *} \right) = \bigcup_{i=1}^{I^{(j)}} \left(X_{ji} \cup X_{ji}^{\mathrm{sym}} \right), \quad X_{ji} = L_{o_{ji}^{\diamondsuit} o_{ji}^{*}} \cap D_j^{\diamondsuit *}. \tag{3.13}$$

The disappearance integrals $\mathscr{Q}_{jk}$ *are evaluated on the domains* $L_{jk} = [v^{(j-1)}, v^{(j)}] \times [v^{(k-1)}, v^{(k)}]$, *whereas the appearance integrals,* $\mathscr{Q}_{ji}^{\diamondsuit}$ *and* $\mathscr{Q}_{ji}^{*}$, *are evaluated on the diagonal strips* $D_j^{\diamondsuit *} = \{(v^{\diamondsuit}, v^*),\ v^{(j-1)} \leqslant v^{\diamondsuit} + v^* \leqslant v^{(j)}\} / \cup_{k=1}^{N} L_{kk}$, *which are symmetric strips with respect to the axis* $v^{\diamondsuit} = v^*$ (*see* $D_4^{\diamondsuit *}$ *in Fig.* 1). *However, the velocity being only piecewise constant in these strips* $D_j^{\diamondsuit *}$, *they are divided into domains, denoted by* X_{ji} *and the symmetric one,* X_{ji}^{sym}, *where the velocity of the partners is constant. The domains* X_{ji} *and* X_{ji}^{sym} *are the intersection of* $D_j^{\diamondsuit *}$ *with* $L_{kl}, k > l$ *and* $L_{kl}, k < l$, *respectively* (3.13); *their index is noted* $i \in [1, I^{(j)}]$ *and we define two pointers which indicate the collision partners for coalescence, at fixed* $i : o_{ji}^{\diamondsuit} = k$ *and* $o_{ji}^{*} = l$.

The source terms due to coalescence conserve mass and momentum:

$$\sum_{j=1}^{N} C_{\mathrm{m}}^{(j)} = 0, \quad \sum_{j=1}^{N} C_{\mathrm{mu}}^{(j)} = 0. \tag{3.14}$$

Remark 3.4. Let us underline that the $\mathscr{Q}$ coefficients only result from the projected coalescence integral operators involved in (3.1) and (3.2) by writing that the form of n is constant in a section an independent on t and x as expressed in Eq. (3.5). It is for this reason that they do not depend themselves neither on t nor x.

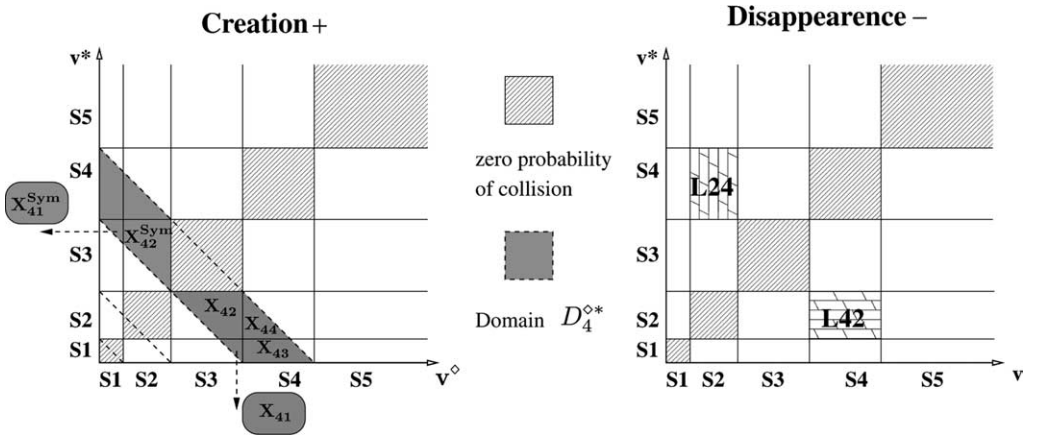

Fig. 1. Diagram of the integration domains for the evaluation of the pre-calculated collisional integrals.

Finally, the coefficients used in the model, either for the evaporation process or the drag force $E_1^{(j)}$, $E_2^{(j)}$ and $\overline{F}^{(j)}$, $j = [1, N+1]$ in (3.6) and (3.7), or for the coalescence: $\mathcal{Q}_{jk}$, $j = [1, N+1], k = [1, N+1], k \neq j$, $\mathcal{Q}_{ji}^{\diamond}$, $\mathcal{Q}_{ji}^{*}$, $j = [2, N+1], i = [1, I^{(j)}]$ in (3.9) and (3.10) can be pre-evaluated from the choice of the droplet size discretization and from the choice of $\kappa^{(j)}$ since the collision integrals do not depend on time nor space. The algorithms for the evaluation of these coefficients are provided in the following section.

Once the coefficients are evaluated, Eqs. (3.6) and (3.7) can be solved using a finite volume method where the fluxes are obtained from a kinetic scheme such as the one developed in [32]. For the purpose of validating the method, we have chosen to focus on a self-similar 2D axisymmetrical configuration in Section 5. This configuration is presented in Section 5.1. In this context, for the stationary case, a simple Eulerian solver can be used and it is presented in Section 5.4. In the non-stationary case, the extension of the finite volume method to the present configuration is detailed in Section 5.4.

Remark 3.5. We did not consider coalescence due to random small velocity differences at the microscopic level nor coalescence due to turbulent agitation. In this case, the link has to be made with, on the one side, the velocity distribution inside the section and on the other side, the local dispersion around the averaged velocity at a given size. In the limit of very small particles like soots, the mean velocity difference with the gaseous phase is zero and the effective velocity difference is due to thermal motion of the gas molecules. It can then be shown that, assuming a Maxwellian velocity distribution at a given size, we retrieve the original formalism of Greenberg et al. [21] but this is beyond the scope of this paper.

4. Precalculation of the various coefficients

For the Eulerian multi-fluid approach, the evaluation of the coalescence source terms can be done from the values of the constant parameters $\mathcal{Q}_{jk}$, $\mathcal{Q}_{ji}^{\diamond}$ and $\mathcal{Q}_{ji}^{*}$. It is the same as for evaporation and drag.

We provide, in this section, a method in order to pre-calculate these constants for a size discretization with $N+1$ sections $[v^{(i-1)}, v^{(j)}[$, with

$$0 = v^{(0)} < v^{(1)} < \cdots < v^{(N)} < v^{(N+1)} = +\infty.$$

In the following, $R^{(j)}$ and $s^{(j)}$ will, respectively, denote the radius and the surface corresponding to the volume $v^{(j)}$.

The distribution function is chosen constant as a function of the radius in sections 1 to N and exponentially decreasing as a function of the surface in the last section [24]. The function $\kappa^{(j)}$, as a function of the radius, the surface or the volume (with $\kappa^{(j)}(R)\,\mathrm{d}R = \kappa^{(j)}(s)\,\mathrm{d}s = \kappa^{(j)}(v)\,\mathrm{d}v$) is then given by, for $j \in \{1,\ldots,N\}$,

$$\kappa^{(j)}(R) = \alpha_j, \quad \kappa^{(j)}(v) = \frac{\alpha_j}{(4\pi)^{1/3}(3v)^{2/3}}, \tag{4.1}$$

and for the last section

$$\kappa^{(N+1)}(s) = \lambda \mathrm{e}^{-\beta(s-s^{(N)})}, \quad \kappa^{(N+1)}(R) = \lambda 8\pi R \mathrm{e}^{-\beta 4\pi\left(R^2-R^{(N)^2}\right),} \tag{4.2}$$

where α_j and λ are such as $\int_{v^{(j-1)}}^{v^{(j)}} \rho_l v \kappa^{(j)}(v)\,\mathrm{d}v = 1$ for $j \in \{1,\ldots,N+1\}$. We then have

$$\alpha_j = \frac{3}{\rho_l \pi (R^{(j)^4} - R^{(j-1)^4})}, \quad \lambda = \frac{6\sqrt{\pi}}{\rho_l}\left(\frac{s^{(N)^{3/2}}}{\beta} + \frac{3\sqrt{s^{(N)}}}{2\beta^2} + \frac{3}{2\beta^{5/2}}J\right)^{-1}, \tag{4.3}$$

where

$$J = \mathrm{e}^{\beta s^{(N)}} \int_{\sqrt{\beta s^{(N)}}}^{+\infty} \mathrm{e}^{-x^2}\,\mathrm{d}x. \tag{4.4}$$

The coefficients $\mathscr{Q}_{jk}$, $\mathscr{Q}_{il}^{\diamondsuit}$ and $\mathscr{Q}_{il}^{*}$ are integrals of the function $g(v,v^*)\kappa^{(j)}(v)\kappa^{(k)}(v^*)$ over different sets, where

$$g(v,v^*) = \rho_l v \pi \left[\left(\frac{3v}{4\pi}\right)^{1/3} + \left(\frac{3v^*}{4\pi}\right)^{1/3}\right]^2.$$

We will then see how to perform this calculations.

4.1. Precalculation of the coalescence collisional integrals: algorithm

4.1.1. Calculation of the destruction collisional integrals

The $\mathscr{Q}_{jk}$ are the integral of $g(v,v^*)\kappa^{(j)}(v)\kappa^{(k)}(v^*)$ over $[v^{(j-1)}, v^{(j)}[\times[v^{(k-1)}, v^{(k)}[$. We use the radius variables, easier for the calculations:

$$\mathscr{Q}_{jk} = \int_{R^{(j-1)}}^{R^{(j)}} \left\{ \int_{R^{(k-1)}}^{R^{(k)}} \kappa^{(j)}(R)\kappa^{(k)}(R^*) g\left(\frac{4}{3}\pi R^3, \frac{4}{3}\pi (R^*)^3\right) \mathrm{d}R^* \right\} \mathrm{d}R. \tag{4.5}$$

This integral depends on the shape of $\kappa^{(j)}$ and $\kappa^{(k)}$. We know that the collision probability between droplets of the same group is zero because they have the same velocity. We then take $\mathscr{Q}_{jj} = 0$. For the other terms, the evaluation procedure is different depending if the last section is involved or not.

j and k less than N. In this case, the $\kappa^{(j)}(R)$ and $\kappa^{(k)}(R)$ are the constants α_j and α_k. The evaluation of the collisional integral yields after some algebra

$$\mathscr{Q}_{j,k} = \alpha_j \alpha_k \rho_l \frac{4}{3}\pi^2 \left\{ \frac{R^{(j)^6} - R^{(j-1)^6}}{6}(R^{(k)} - R^{(k-1)}) + \frac{R^{(j)^5} - R^{(j-1)^5}}{5}(R^{(k)^2} - R^{(k-1)^2}) + \left(\frac{R^{(j)^4} - R^{(j-1)^4}}{4}\right)\left(\frac{R^{(k)^3} - R^{(k-1)^3}}{3}\right) \right\}. \tag{4.6}$$

k = N+1 or j = N+1. In this case, one of the $\kappa^{(j)}$ and $\kappa^{(k)}$ is exponentially decreasing at infinity. Because the function g is not symmetric, we have to calculate the two coefficients. As a function of integral J defined by (4.4), we obtain

$$\mathscr{Q}_{j,N+1} = \alpha_j \rho_l \frac{4\pi^2\lambda}{3\beta}\left\{\frac{R^{(j)^6} - R^{(j-1)^6}}{6} + \frac{R^{(j)^4} - R^{(j-1)^4}}{4}\left(R^{(N)^2} + \frac{1}{4\pi\beta}\right) + \frac{R^{(j)^5} - R^{(j-1)^5}}{5}\left(2R^{(N)} + \frac{J}{\sqrt{\pi\beta}}\right)\right\}, \tag{4.7}$$

$$\begin{aligned}\mathscr{Q}_{N+1,k} = \alpha_k \frac{\rho_l\lambda}{3\beta^3}\Bigg\{&(R^{(j)} - R^{(j-1)})\left[4\pi^2\beta^2 R^{(N)^5} + \frac{5}{2}\pi\beta R^{(N)^3} + \frac{15R^{(N)}}{16} + \frac{15J}{32\sqrt{\pi\beta}}\right]\\ &+ (R^{(j)^2} - R^{(j-1)^2})\left[4\pi^2\beta^2 R^{(N)^4} + 2\pi\beta R^{(N)^2} + \frac{1}{2}\right]\\ &+ \frac{R^{(j)^3} - R^{(j-1)^3}}{3}\left[4\pi^2\beta^2 R^{(N)^3} + \frac{3\pi\beta}{2}R^{(N)} + \frac{3\sqrt{\pi\beta}}{4}J\right]\Bigg\}.\end{aligned} \tag{4.8}$$

We only need to numerically evaluate the integral J. It can be made for example with a Simpson method, the integral $\int_a^{+\infty} e^{-x^2}\,dx$ being approached by $\int_a^{a+b} e^{-x^2}\,dx$ with b sufficiently large and then a precision higher than e^{-b^2}.

4.1.2. Calculation of $\mathscr{Q}_{ji}^{\diamondsuit}$ and $\mathscr{Q}_{ji}^{*}$

It has to be mentioned that we adopt here the opposite point of view as the one presented in Section 3.2, where we were looking for the set of intersection, for a given section, of the corresponding diagonal strip with all the rectangles where the velocity field is constant. In this paragraph, we consider a given rectangle L_{jk} with $j < k$, because of symmetry, and we will find all the diagonal strips intersecting with it. It will allow us to calculate all the collisional integrals and then to construct the pointers $o_{ji}^{\diamondsuit}$ and o_{ji}^{*}.

For each rectangle L_{jk}, we locate the $D_i^{\diamondsuit *}$ which intersects L_{jk}, that is $D_i^{\diamondsuit *}$ for $i \in [i_{\min}, i_{\max}+1]$ such that $i_{\min}$ is the minimum of $\{i \in \mathbb{N}, v^{(j-1)} + v^{(k-1)} < v^{(i)}\}$ and $i_{\max}$ is the maximum of $\{i \in \mathbb{N}, v^{(i)} < v^{(j)} + v^{(k)}\}$. We then define $X_{il} = L_{jk} \cap D_i^{\diamondsuit *}$ where $l-1$ is the number of preceding rectangle which intersects $D_i^{\diamondsuit *}$. We have also the value for the pointers: $o_{il}^{\diamondsuit} = j$ and $o_{il}^{*} = k$.

If only one $D_i^{\diamondsuit *}$ intersects L_{jk} ($i_{\min} = i_{\max} + 1$), then $\mathscr{Q}_{il}^{\diamondsuit} = \mathscr{Q}_{jk}$ and $\mathscr{Q}_{il}^{*} = \mathscr{Q}_{kj}$. In the other cases, we obviously have $j \leqslant N$ and $k \leqslant N$ so that $\kappa^{(j)}$ and $\kappa^{(k)}$ are given by (4.1). We will also decompose the set in which we have to make the integral in rectangles and triangles (in the volume phase space).

We then have to calculate the integral of $\frac{g(v,v^*)}{(4\pi)^{2/3}3^{4/3}v^{2/3}(v^*)^{2/3}}$ over three kinds of sets:

- rectangle $[v_1, v_2] \times [v_1^*, v_2^*]$ (this integral is noted $\mathscr{R}(v_1, v_2, v_1^*, v_2^*)$),
- lower isosceles triangles $\{(v, v^*), v_0 \leqslant v \leqslant v_0 + \Delta v, v_0^* \leqslant v^* \leqslant v_0 + v_0^* + \Delta v - v\}$ (this integral is noted $LT(v_0, v_0^*, \Delta v)$),
- upper isosceles triangles $\{(v, v^*), v_0 - \Delta v \leqslant v \leqslant v_0, v_0 + v_0^* - \Delta v - v \leqslant v^* \leqslant v_0^*\}$ (this integral is noted $UT(v_0, v_0^*, \Delta v)$),

where we have denoted $\mathscr{Q}_{jk} = \alpha_j\alpha_k\mathscr{R}(v^{(j-1)}, v^{(j)}, v^{(k-1)}, v^{(k)})$, where the function $\mathscr{R}$ is given in the previous subsection by (4.6).

LT and UT are given by:

$$LT(v_0, v_0^*, \Delta v) = \frac{\rho_l 3^{1/3}}{4^{4/3}\pi^{1/3}} \left\{ \frac{3}{4} v_0 (v_0^* + \Delta v)^{4/3} - \frac{3}{4}(v_0 + \Delta v)(v_0^*)^{4/3} - \frac{9}{28}(v_0^*)^{7/3} + \frac{9}{28}(v_0^* + \Delta v)^{7/3} + \frac{1}{2}[(v_0 + \Delta v)^2 - v_0^2](v_0^*)^{1/3} - \frac{3}{5}[(v_0 + \Delta v)^{5/3} - v_0^{5/3}](v_0^*)^{2/3} + \frac{3}{28}(v_0 + \Delta v)^{7/3} + \frac{1}{4}(v_0 + \Delta v)v_0^{4/3} + \frac{1}{7}v_0^{7/3} + \int_0^{\Delta v} (v + v_0)^{2/3}(v_0^* + \Delta v - v)^{2/3} \mathrm{d}v \right\}, \tag{4.9}$$

$$UT(v_0, v_0^*, \Delta v) = \frac{\rho_l 3^{1/3}}{4^{4/3}\pi^{1/3}} \left\{ \frac{3}{4} v_0 (v_0^* - \Delta v)^{4/3} - \frac{3}{4}(v_0 - \Delta v)(v_0^*)^{4/3} - \frac{9}{28}(v_0^*)^{7/3} + \frac{9}{28}(v_0^* - \Delta v)^{7/3} + \frac{1}{2}[v_0^2 - (v_0 - \Delta v)^2](v_0^*)^{1/3} - \frac{3}{5}[v_0^{5/3} - (v_0 - \Delta v)^{5/3}](v_0^*)^{2/3} + \frac{3}{28}(v_0 - \Delta v)^{7/3} + \frac{1}{4}(v_0 - \Delta v)v_0^{4/3} + \frac{1}{7}v_0^{7/3} - \int_0^{\Delta v} (v + v_0 - \Delta v)^{2/3}(v_0^* - v)^{2/3} \mathrm{d}v \right\}. \tag{4.10}$$

Only a simple integral have to be numerically calculated for each calculation of LT or UT.

We can then evaluate I_{jk}^i, the integral of $g(v, v^*)\kappa^{(j)}(v)\kappa^{(k)}(v^*)$ over $[v^{(j-1)}, v^{(j)}) \times [v^{(k-1)}, v^{(k)}[\cap\{(v, v^*), v + v^* \leqslant v^{(i)}\}$. We will then have $\mathcal{Q}_{il}^{\diamondsuit} = I_{jk}^i - I_{jk}^{i-1}$, if $I_{jk}^0 = 0$. In the same way, we can define I_{kj}^i and we will have: $\mathcal{Q}_{il}^* = I_{kj}^i - I_{kj}^{i-1}$.

We can remark that $I_{jk}^{i_{\max}+1} = \mathcal{Q}_{jk}$. In order to calculate the I_{jk}^i for $i \in [i_{\min}, i_{\max}]$, we distinguish areas bordered by the lines $v + v^* = a$, $v + v^* = b$ and the boundaries of the rectangle, where $a = v^{(j-1)} + v^{(k)}$ and $b = v^{(j)} + v^{(k-1)}$ (see Fig. 2). Four cases have to be considered, according to the position of the line $v + v^* = v^{(i)}$ with respect to the areas 1, 2, 2' or 3:

- if $v^{(i)} \leqslant a$ and $v^{(i)} \leqslant b$ (area 1) then $I_{jk}^i = \alpha_j \alpha_k LT(v^{(j-1)}, v^{(k-1)}, v^{(i)} - v^{(j-1)} - v^{(k-1)})$,
- if $a < v^{(i)} < b$ (area 2, example in Fig. 2) then $I_{jk}^i = \alpha_j \alpha_k \{R(v^{(j-1)}, v^{(i)} - v^{(k)}, v^{(k-1)}, v^{(k)}) + LT(v^{(i)} - v^{(k)}, v^{(k-1)}, v^{(k)} - v^{(k-1)})\}$,
- if $b < v^{(i)} < a$ (area 2', example in Fig. 2) then $I_{jk}^i = \alpha_j \alpha_k \{R(v^{(j-1)}, v^{(j)}, v^{(k-1)}, v^{(i)} - v^{(j)}) + LT(v^{(j-1)}, v^{(i)} - v^{(j)}, v^{(j)} - v^{(j-1)})\}$,

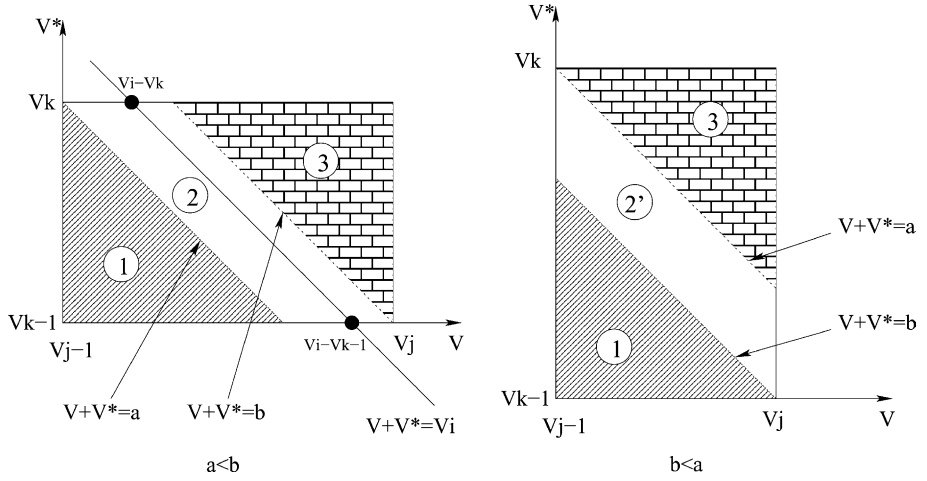

Fig. 2. Various intersection possibilities of diagonal strips and rectangles.

- if $v^{(i)} \geqslant a$ and $v^{(i)} \geqslant b$ (area 3) then $I^i_{jk} = \mathscr{Q}_{j,k} - \alpha_j \alpha_k UT(v^{(j)}, v^{(k)}, v^{(j)} + v^{(k)} - v^{(i)})$,

I^i_{kj} is given by the same formulae by changing j and k, in the four cases.

So far, we have obtained the values of $\mathscr{Q}_{jk}$, $\mathscr{Q}^{\diamondsuit}_{il}$ and $\mathscr{Q}^{*}_{il}$ and of the pointers $o^{\diamondsuit}_{il} = j$ and $o^{*}_{il} = k$.

4.2. Precalculation of the evaporation coefficients and mean drag

4.2.1. Calculation of the evaporation coefficients

In the context of the chosen configuration defined by equation (5.1), we get the following expressions for the evaporation coefficients $E^{(j)}_1$ and $E^{(j)}_2$, $j \leqslant N$:

$$E^{(j)}_1 = -\rho_l v^{(j-1)} \kappa^{(j)}(t,x,v^{(j-1)}) R_v(t,x,v^{(j-1)}) = -\frac{1}{\pi} \frac{R^{(j-1)}}{{R^{(j)}}^4 - {R^{(j-1)}}^4} R_v(t,x,v^{(j-1)}), \tag{4.11}$$

$$E^{(j)}_2 = -\rho_l \int_{v^{(j-1)}}^{v^{(j)}} \kappa^{(j)}(t,x,v)\, R_v(t,x,v)\, \mathrm{d}v = -\frac{3}{\pi} \frac{R^{(j)} - R^{(j-1)}}{{R^{(j)}}^4 - {R^{(j-1)}}^4} R_v(t,x,v^{(j)}_{moy}), \tag{4.12}$$

where the mean evaporation volume is given by:

$$v^{(j)}_{moy} = \frac{4}{3}\pi {R^{(j)}_{moy}}^3, \qquad R^{(j)}_{moy} = \frac{R^{(j)} + R^{(j-1)}}{2}, \tag{4.13}$$

since R_v is proportional to the radius with the use of the d^2 law. For the last section, where $\kappa^{(N+1)}(s) = \lambda \mathrm{e}^{-\beta(s - s^{(N)})}$, we obtain:

$$E^{(N+1)}_1 = -\frac{4\sqrt{\pi} s^{(N)}}{\frac{{s^{(N)}}^{3/2}}{\beta} + \frac{3\sqrt{s^{(N)}}}{2\beta^2} + \frac{3}{2}\frac{J}{\beta^{5/2}}} R_v(t,x,v^{(N)}), \tag{4.14}$$

$$E^{(N+1)}_2 = -\frac{6\sqrt{\pi}}{{s^{(N)}}^{3/2} + \frac{3\sqrt{s^{(N)}}}{2\beta} + \frac{3}{2}\frac{J}{\beta^{3/2}}} R_v(t,x,v^{(N+1)}_{moy}), \tag{4.15}$$

where J has been defined by Eq. (4.4) and where the mean evaporation volume reads:

$$v^{(N+1)}_{moy} = \frac{4}{3}\pi\, {R^{(N+1)}_{moy}}^3, \qquad R^{(N+1)}_{moy} = R^{(N)} + \frac{J}{2\sqrt{\pi\beta}}. \tag{4.16}$$

4.2.2. Calculation of the mean drag

The expression of the mean drag force in the jth section is given by:

$$F^{(j)} = \int_{v^{(j-1)}}^{v^{(j)}} \rho_l v \overline{F}(t,x,v) \kappa^{(j)}(v)\, \mathrm{d}v = \overline{F}(t,x,v^{(j)}_u), \tag{4.17}$$

where the mean drag volume $v^{(j)}_u$, $j \leqslant N$, reads:

$$v^{(j)}_u = \frac{4}{3}\pi {R^{(j)}_u}^3, \qquad R^{(j)}_u = \sqrt{\frac{{(R^{(j)})}^2 + {(R^{(j-1)})}^2}{2}}, \tag{4.18}$$

since the Stokes drag coefficient is proportional to the inverse of the radius to the square. For the last section, we obtain:

$$v_u^{(N+1)} = \frac{4}{3}\pi R_u^{(N+1)^3}, \qquad R_u^{(N+1)^2} = \frac{R^{(N)^3} + \frac{3R^{(N)}}{8\pi\beta} + \frac{3J}{16\pi^{3/2}\beta^{3/2}}}{R^{(N)} + \frac{J}{2\sqrt{\pi\beta}}}. \tag{4.19}$$

The Eulerian multi-fluid conservation equations governing the spray can then be resolved.

5. Validation through a reference Lagrangian solver: the nozzle test-case

This section is devoted to a representative test-case in both stationary and unstationary configurations: a decelerating self-similar 2D axisymmetrical nozzle. The details of the test-case and of the characteristics parameters of the three injected sprays with various size distributions are provided in the first subsection. The solvers for both the Lagrangian reference solution and the Eulerian multi-fluid method are then presented as well as the information of the various parameters involved with both methods. The Eulerian multi-fluid model is then validated in comparison with the Lagrangian solver and the influence of the level of refinement in the size discretization is studied. Finally the validity of the assumption on velocity dispersion underlying the Eulerian model and the computational efficiency of this approach, in comparison to the Lagrangian approach, is investigated.

5.1. Definition of configuration

We conduct numerical simulations with both Lagrangian and Eulerian solvers on the test-case configuration of a conical diverging nozzle. This configuration is originally unstationary 2D axisymmetrical in space and 1D in droplet size and can be considered as representative of the difficulty one is going to encounter in realistic problems since it involves a 3D unstationary calculation. However, we are not going to precisely evaluate all the properties of the spray as in [1,8] and [24].

The purpose of the comparison is to prove on the one side the ability of the Eulerian multi-fluid model to correctly describe the coalescence phenomenon and on the other side to provide a comparison tool for the numerical simulations based on Lagrangian models and solvers in terms of precision and CPU cost. Consequently, we only consider simple droplet models as already mentioned in Section 2.1.

A spray of pure heptane fuel is carried by a gaseous mixture of heptane and nitrogen into a conical diverging nozzle. At the entrance, 99% of the mass of the fuel is in the liquid phase, whereas 1% is in the gaseous mixture. The mass fraction in the gas are then respectively of 2.9% for heptane and 97.1% for the nitrogen. The temperature of the gas mixture is supposed to be fixed during the whole calculation at 400 K. The influence of the evaporation process on the gas characteristics is not taken into account in our one-way coupled calculation. It is clear that the evaporation process is going to change the composition of the gaseous phase and then of the evaporation itself. However, we do not want to achieve a fully coupled calculation, but only to compare two ways of evaluating the coupling of the dynamics, evaporation and coalescence of the droplets. It has to be emphasized that it is not restrictive in the framework of this study which is focused on the introduction, validation and cost evaluation of a new Eulerian solver for the liquid phase.

In order to only solve for stationary and unstationary problems as a 1D problem in space and 1D problem in droplet size, we make a similarity assumption on the gas and droplets variables. Actually, we choose a stationary gas flow in the conical nozzle such that the axial velocity does not depend on the radial coordinate r and such that the radial velocity is linear as a function of the radial coordinate, whereas the linearity coefficient does not depend on r:

$$v_z = V(z), \quad v_r = rU(z). \tag{5.1}$$

In this stationary configuration of an incompressible flow, we can determine the velocity field given by $(V(z), U(z))$ such that the stream lines are straight:

$$V(z) = \frac{z_0^2 V(z_0)}{z^2}, \quad U(z) = \frac{V(z)}{z} = \frac{z_0^2 V(z_0)}{z^3}, \tag{5.2}$$

where $z_0 > 0$ is fixed as well as $V(z_0)$. The trajectories of the fluid particles are then given by

$$r(t) = r(0)\left(1 + \frac{3V(z_0)}{z_0}t\right)^{1/3}, \quad z(t) = z(0)\left(1 + \frac{3V(z_0)}{z_0}t\right)^{1/3}.$$

As for the droplets, we also assume similarity; their trajectories are straight if their injection velocity is colinear to the one of the gas (see Fig. 3). The similarity assumption is only valid when no coalescence is to be found. However, even in the presence of coalescence, it is verified in a neighborhood of the central line.

Let us finally consider three droplet distribution functions. The first one, called monomodal, is composed of droplets with radii between 0 and 35 μm, with a Sauter mean radius of 15.6 μm and a variance of $D_{10} = 24$ μm. It is represented in Fig. 4 and is typical of the experimental condition reported in [24]. The droplets are only constituted of liquid heptane, their initial velocity is the one of the gas, their initial temperature, fixed at the equilibrium temperature 325.4 K (corresponding to an infinite conductivity model), does not change along the trajectories. The second one is constant as a function of radius on the interval [15 μm, 30 μm] and zero elsewhere. It is then discontinuous and represent a first step into the treatment of non-smooth distributions. It will be the one we will use for the unsteady calculations. The third distribution is called bimodal since it involves only two groups of radii, respectively, 10 μm and 30 μm with equivalent mass density. This bimodal distribution function is typical of alumina particles in solid propergol rocket boosters [2]. It is represented in Fig. 4 and is probably the most difficult test case for a Eulerian description of the size phase space.

The initial injected mass density is then taken at $m_0 = 3.609$ mg/cm^3 so that the volume fraction occupied by the liquid phase is 0.57% in the stationary case and fluctuates around this value in the unstationary one. Because of the deceleration of the gas flow in the conical nozzle, droplets are going to also decelerate, however at a different rate depending on their size and inertia. This will induce coalescence. The deceleration at the entrance of the nozzle is taken at $a(z_0) = -2(V(z_0)/z_0)$; it is chosen large enough so that the velocity difference developed by the various sizes of droplets is important. In the stationary configuration, we have chosen a very large values as well as a strong deceleration leading to extreme cases: $V(z_0) = 5$ m/s,

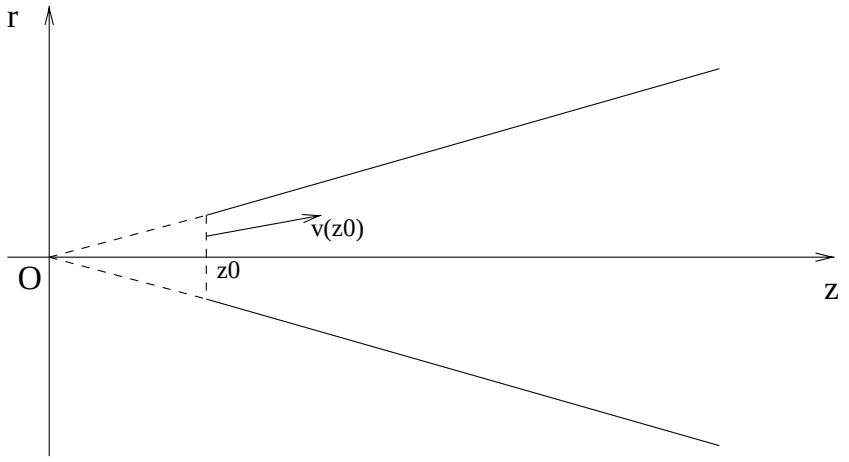

Fig. 3. Sketch of the conical diverging nozzle.

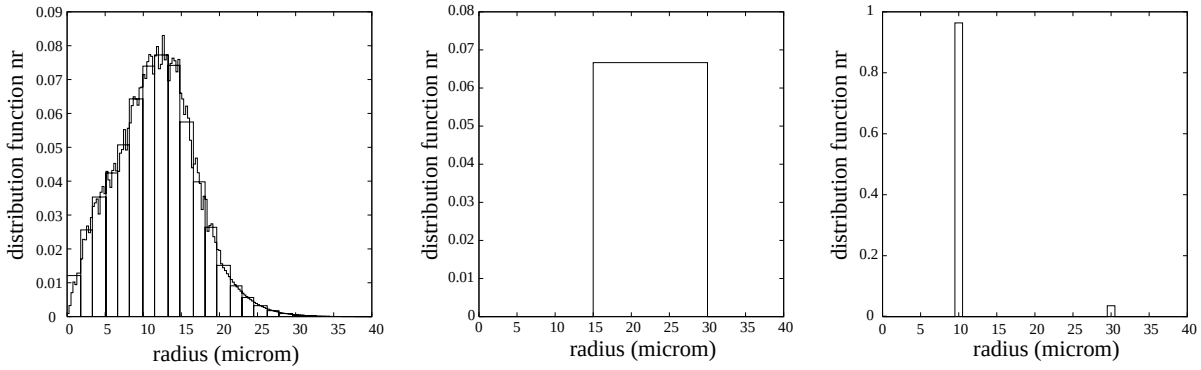

Fig. 4. (left) Monomodal distribution function from experimental measurements and 30 section discretization, (middle) discontinuous distribution function, (right) bimodal distribution function discretized with 50 sections.

$z_0 = 10$ cm for the monomodal case and $V(z_0) = 5$ m/s, $z_0 = 5$ cm for the bimodal case. It generates a very strong coupling of coalescence and dynamics and induces an important effect on the evaporation process; it is a good test-case for the Eulerian model. We have chosen a case a little less drastic in the unsteady configuration: $z_0 = 20$ cm and $V(z_0) = 4$ m/s. In this case, the mass density of the droplets who are injected at the entrance of the nozzle $z = z_0$ varies with time: the total mass density m at this point is given by

$$m(t, z_0) = [1 + 0.9\sin(\omega t)]m_0,$$

where $\omega = 390\ \mathrm{s}^{-1}$ and the oscillations occurs around the total mass density for the stationary case m_0. Because of these oscillations, the coalescence phenomenon is affected, and this effect, coupled to the dynamics of the droplets, results in strong oscillations in the Sauter mean diameter and mean velocity of the spray. It will prove to be a difficult test-case, even for the Lagrangian solver, and all the more for the Eulerian one.

Before coming to the result sub-section and before comparing the methods for various distributions, let us present the two solvers.

5.2. A reference Lagrangian solver

Euler–Lagrange numerical methods are commonly used for the calculation of polydisperse sprays in various application fields (see for example [10,14,30,36] and the references therein). In this kind of approach, the gas phase is generally computed with a finite volume Eulerian solver, while the dispersed phase is treated with a random particle method. The influence of the droplets on the gas flow is taken into account by the presence of source terms in the r.h.s. of the Navier–Stokes (or Euler) equations.

A complete exposition on the derivation and the implementation of such a method is out the scope of this paper. We refer, for example, to [11,30] or [2] for more details. Here, for the sake of completeness, we present the main features of the numerical method that we used in order to provide a ''reference numerical solution''.

A particle method can be interpreted as a direct discretization of the kinetic Eq. (2.1). At each time step, the droplet distribution function $f(t^k)$ is approximated by a finite weighted sum of Dirac masses, $\tilde{f}(t^k)$, which reads

$$f(t^k) = \sum_{i=1}^{N^k} n_i^k \delta_{z_i^k, u_i^k, v_i^k}. \tag{5.3}$$

Each weighted Dirac mass is generally called a ''parcel'' and can be physically interpreted as an aggregated number of droplets (the weight n_i^k), located around the same point, x_i^k, with about the same ve-

locity, u_i^k and about the same volume, v_i^k. N^k denotes the total number of parcels in the computational domain, at time t^k. In all our calculations, the weights n_i^k were chosen in such a way that each parcel represents the same volume of liquid ($n_i^k v_i^k = \text{Const.}$).

Each time step of the particle method is divided in two stages. The first one is devoted to the discretization of the l.h.s. of the kinetic Eq. (2.1), modeling the motion and evaporation of the droplets. In our code, the new position, velocity and volume of each parcel are calculated according to the following numerical scheme:

$$\begin{cases} u_i^{k+1} = u_i^k \exp(-\Delta t/\tau_i^k) + V(z_i^k)(1 - \exp(-\Delta t/\tau_i^k)), \\ v_i^{k+1} = \frac{4\pi}{3} \max\left(0, \left[\left(\frac{3v_i^k}{4\pi}\right)^{2/3} - E\Delta t\right]\right)^{3/2}, \\ z_i^{k+1} = z_i^k + \Delta t V(z_i^k) + (u_i^k - V(z_i^k)\exp(-\Delta t/\tau_i^k)), \end{cases} \tag{5.4}$$

where V denotes the axial gas velocity, E is the constant of the evaporation model ($E = 1.583\ 10^{-8}$ m^2/s), z_i^k – respectively u_i^k – corresponds to the axial coordinate of the position – respectively of the velocity – of the parcel i at time and τ_i^k is the parcel relaxation time defined as

$$\tau_i^k = \frac{2\rho_l (r_i^k)^2}{9\mu_g},$$

with r_i^k being the parcel radius, ρ_l the liquid density and μ_g the gas viscosity.

In system (5.4), the parcel radial coordinate is not calculated, in order to keep the same hypothesis as for the 1D multi-fluid Eulerian model. Besides, as mentioned above, the influence of the droplets on the gas flow is not taken into account. Hence, Eq. (5.2) is used to calculate the gas velocity, $V(z_i^k)$ at the parcel location.

The second stage of a time step is devoted to the discretization of the collision operator. A lot of Monte-Carlo algorithms have been proposed in the literature for the treatment of droplet collisions ([2,10,14,30,37]). They are all inspired by the methods used in molecular gas dynamics [38] and, in particular, they suppose that the computational domain is divided into cells, or control volumes, which are small enough to consider that the droplet distribution function is almost uniform over them.

The algorithm used in our reference Lagrangian solver is close to the one proposed by O'Rourke. It consists of the following three steps (see also [30] for more details).

1. For each computational cell C_J, containing N_J parcels, we choose randomly, with a uniform distribution law, $N_J/2$ pairs of parcels ($(N_J - 1)/2$, if N_J is odd).
2. For each pair p, let p_1 and p_2 denote the two corresponding parcels with the convention $n_1 \geqslant n_2$, where n_1 and n_2 denote the parcel numerical weights. Then for each pair p of the cell C_J, we choose randomly an integer v_p, according to the Poisson distribution law

$$P(v) = \frac{\lambda_{12}}{v!} \exp(-\lambda_{12}),$$

with

$$\lambda_{12} = \pi \frac{n_1 (N_J - 1)\Delta t}{\text{vol}(C_J)} (R_1 + R_2)^2 |u_1 - u_2|$$

with $\text{Vol}(C_J)$ being the volume of the cell C_J (proportional to $(z_J/z_0)^2$ for the nozzle test case problem) and R_1, R_2 being the radii of the parcels p_1, p_2. The coefficient λ_{12} represents the mean number of collision, during $(N_j - 1)$ time steps, between a given droplet of the parcel p_2 and any droplet of the parcel p_1. Note that a given pair of parcels is chosen, in average, every $(N_j - 1)$ time steps.

3. If $v_p = 0$, no collision occurs during this time step between the parcels p_1 and p_2. Otherwise, if $v_p > 0$, the parcel p_1 undergoes v_p coalescences with the parcel p_2 and the outcome of the collision is treated as follows. First the weight n_1 of the parcel p_1 is replaced by $n_1' = n_1 - n_2$ and its other characteristics are left unchanged. If $n_1' \leqslant 0$, the parcel p_1 is removed from the calculation. Secondly, the velocity u_2 and the volume v_2 of the parcel p_2 are replaced by

$$v_2' = v_2 + v_p v_1, \quad u_2' = \frac{v_2 u_2 + v_p v_1 u_1}{v_2 + v_p v_1},$$

and its weight, n_2, is left unchanged.

Let us mention that, for each time step and each control volume C_J, the computational cost of this algorithm behaves like $O(N_J)$. This is a great advantage compare to O'Rourke method, which behaves like $O(N_J^2)$. Another algorithm, with the same features, has been recently introduced by Schmidt and Rudtland in [37].

To obtain a good accuracy, the time step, Δt, must be chosen small enough to ensure that the number of collisions between two given parcels, p_1 and p_2, is such that for almost every time: $v_p n_2 \leqslant n_1$. The average value of v_p being λ_{12}, this constraint is equivalent to the condition

$$\frac{n_2 N_J \Delta t}{\mathrm{vol}(C_J)} \pi (R_1 + R_2)^2 |u_1 - u_2| \ll 1. \tag{5.5}$$

For the nozzle test case described above, this constraint reveals to be less restrictive than the "CFL" like condition

$$\forall i = 1, \ldots, N, \quad \frac{|u_i| \Delta t}{\Delta z} \ll 1, \tag{5.6}$$

with Δz being the mesh size. This condition is necessary to compute accurately the droplet movement and in particular to avoid that a parcel goes through several control volumes during the same time step. This is essential to have a good representation of the droplet distribution function in each mesh cell.

5.3. Characteristic computation parameters, reference solutions

Out of the calculations performed in the stationary and unstationary configurations, we have selected two stationary, with the monomodal and bimodal distributions, and one unstationary configuration with the second size distribution which is constant in some size interval and thus possesses two discontinuities. This choice will be shown to be the right one in order to illustrate the main points we want to make in the present paper. The numerical parameters used in order to compute the reference solutions with the Lagrangian approach are summarized in Table 1.

In the stationary configuration, in order to eliminate the numerical noise intrinsic to the Lagrangian approach, time averages (over a period of 0.6 s) have been used to calculate the mass density, the Sauter

Table 1
Parameters for the reference solution

	No. of parcels	No. of parcels inj./s	Δz (m)	Δt (s)
Mon. Stat.	14,000	–	2.5×10^{-3}	1.25×10^{-5}
Bim. Stat.	63,000	–	1.8×10^{-3}	0.9×10^{-5}
Lag. Unst. 1	245,000	5,000,000	3.0×10^{-3}	1.0×10^{-5}
Lag. Unst. 2	49,500	1,000,000	3.0×10^{-3}	1.0×10^{-5}
Lag. Unst. 3	5000	100,000	3.0×10^{-3}	1.2×10^{-5}

mean radius and the mean velocity of the droplets in each computational cell, once the steady state has been reached since the calculations are done with an unsteady really 2D axisymmetrical code. The number of particles present in the domain has been checked to be high enough in order to get a converged solution.

Let us now analyze the main features of the obtained stationary solutions for both initial droplet size distribution. It can be easily seen, in Figs. 5 and 6, that the influence of the coalescence phenomenon is important in both the monomodal and bimodal configurations. Since the droplets of various sizes develop a velocity difference reaching 1 m/s due to the deceleration in the monomodal case, coalescence takes place and changes the profile of the size distribution function and consequently influences the evaporation process by transferring some mass from the small droplets into the big ones. It can also be seen in Fig. 5 that the influence on the Sauter mean diameter can reach five to seven microns in the monomodal case. This demonstrates that the coalescence phenomenon really plays a crucial role in this configuration and is

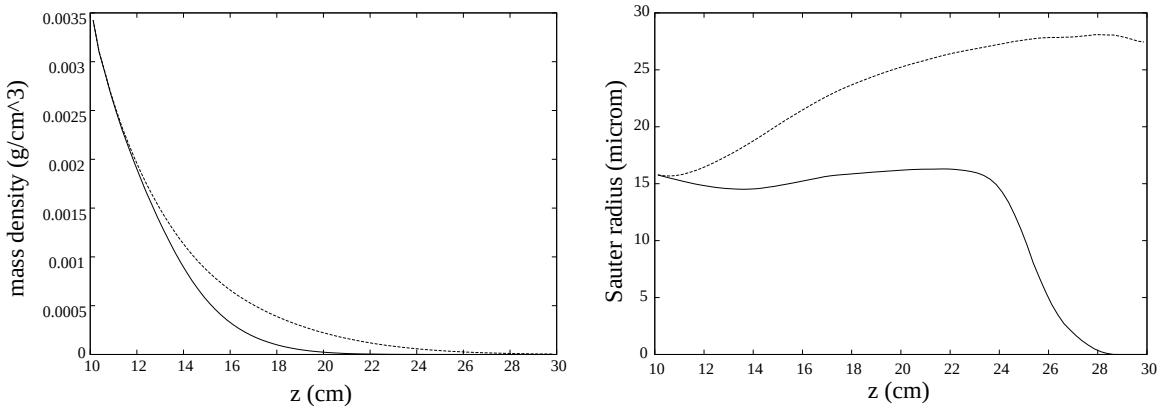

Fig. 5. (left) Evolution of the mass density of liquid for the Lagrangian reference solution with (dashed line) and without (solid line) coalescence for the monomodal case, (right) evolution of the Sauter mean radius of the spray size distribution with (dashed line) and without (solid line) coalescence for the monomodal case.

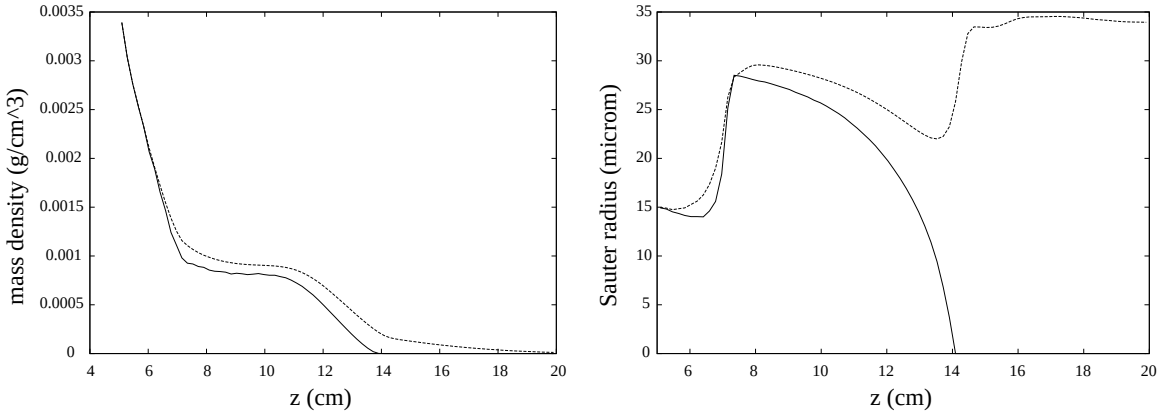

Fig. 6. (left) Evolution of the mass density of liquid for the Lagrangian reference solution with (dashed line) and without (solid line) coalescence for the bimodal case, (right) evolution of the Sauter mean radius of the spray size distribution with (dashed line) and without (solid line) coalescence for the bimodal case.

strongly coupled to the dynamics and evaporation of the spray, thus offering a good test-case in order to validate the multi-fluid Eulerian model.

For most stationary configurations, it is clear that the Lagrangian approach is going to be much more efficient and precise that any Eulerian one. These configurations are only chosen in order to validate the Eulerian model and numerical method introduced in this paper; we will not compare the CPU times, all the more since the codes used in order to get these stationary solutions have a completely different structure.

For the unstationary case, stationary calculation are first performed between the times 0 (where nothing is to be found in the computational domain) and 0.3222 s in order to reach the stationary case. Then, mass density oscillations are introduced. The instantaneous values are given for a time $t = 0.41$ s, in the middle of the sixth period after the beginning of the oscillations. In fact, it is a temporal averaging on a short time interval of 0.5 ms around this value. We are also interested in the temporal averages since the configuration is statistically stationary. This averaging begins after the transition period, when the periodic regime is reached in all the computational domain, that is 10 periods after the beginning of the oscillations at the injection point. Moreover the averaging is done on an interval of 10 oscillations for the Lagrangian method in order to have good statistics with a reasonable number of droplets.

The question of the CPU time becomes more important in this unsteady case. Therefore, we present, in Figs. 7–9, the results obtained with three levels of precision (see Table 1) for the Lagrangian solver and compare the reduced CPU time to the one obtained with the lowest number of particles in the case without coalescence. We obtain: 1.6, for the case Lag. Unst. 3, 23, for the case Lag. Unst. 2, and 123, for the case Lag. Unst. 1. It becomes clear that the case with the lowest number of particles is going to generate artificial fluctuations associated with the Lagrangian description; in the particular applications related to combustion problems, the presence of too few droplets, the vaporization of which is going to create strong spatial and temporal fluctuations in the fuel gaseous mass fraction is going to be as crucial issue. Thus, even if the global qualitative behavior of the spray is reproduced in simulation Lag. Unst. 1 and the reduced CPU time is small, the acceptable level of convergence is not reached. A first acceptable level of convergence is reached for the simulation Lag. Unst. 2. The solution considered as converged and which will be taken as the ''reference solution'' in the following for this unsteady case is Lag. Unst. 3. It is interesting to note that, even if the problem is essentially monodimensional in the space variable, the unsteady character of the

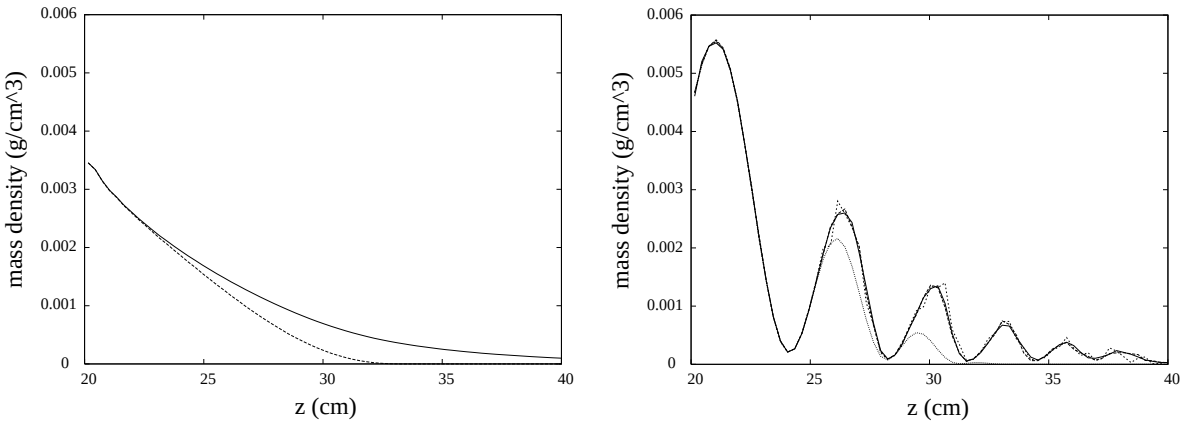

Fig. 7. (left) Evolution of the temporal averaging of the liquid mass density for the Lagrangian reference solution with (solid line) and without (dashed line) coalescence, for the unstationary case, (right) evolution of the mass density of the liquid at $t = 0.41$ s for the three Lagrangian solutions with coalescence (solid line: Lag. Unst. 1, i.e. reference solution; dashed line: Lag. Unst. 2; dotted line: Lag. Unst. 3) and for the Lagrangian reference solution without coalescence (small dotted line).

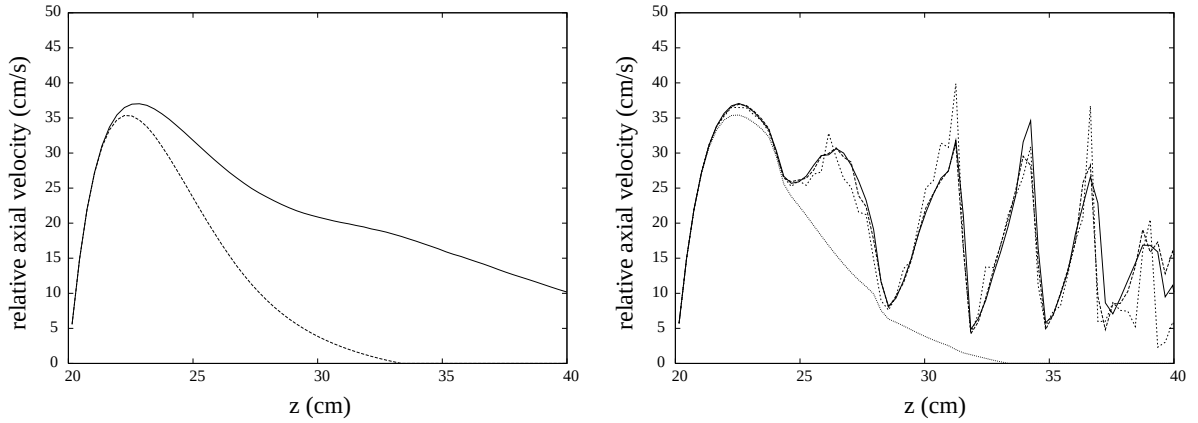

Fig. 8. (left) Evolution of the temporal averaging of the axial mean velocity difference of the liquid phase for the Lagrangian reference solution with (solid line) and without (dashed line) coalescence, for the unstationary case, (right) evolution of the axial mean velocity difference of the liquid at $t = 0.41$ s for the three Lagrangian solutions with coalescence (solid line: Lag. Unst. 1, i.e. reference solution; dashed line: Lag. Unst. 2; dotted line: Lag. Unst. 3) and for the Lagrangian reference solution without coalescence (small dotted line).

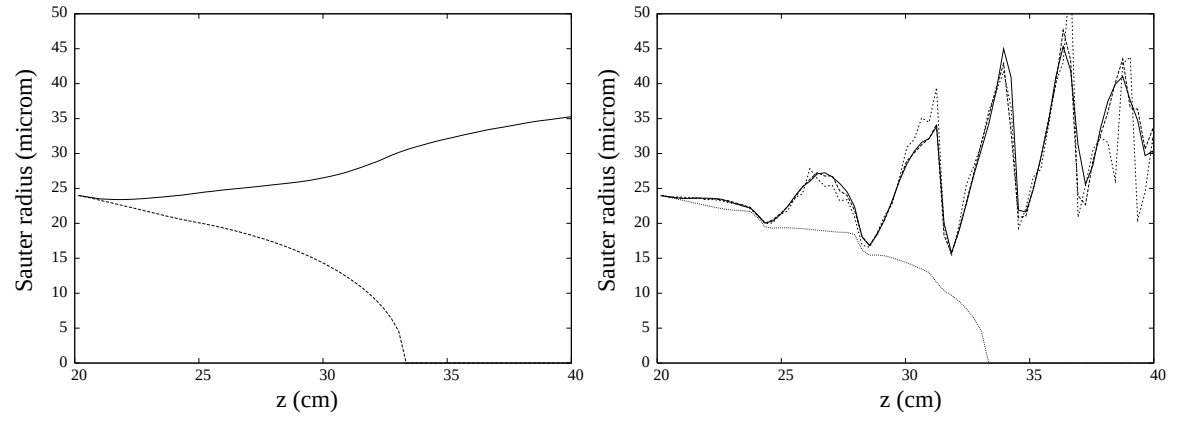

Fig. 9. (left) Evolution of the temporal averaging of the Sauter mean radius of the liquid phase for the Lagrangian reference solution with (solid line) and without (dashed line) coalescence, for the unstationary case, (right) evolution of the Sauter mean radius of the liquid at $t = 0.41$ s for the three Lagrangian solutions with coalescence (solid line: Lag. Unst. 1, i.e. reference solution; dashed line: Lag. Unst. 2; dotted line: Lag. Unst. 3) and for the Lagrangian reference solution without coalescence (small dotted line).

configuration requires a substantial amount of droplets for the solution to be converged, which suggest what is should be for a 2D or 3D problem.

The results are presented, in Figs. 7–9, through the mass density, the Sauter mean radius and the velocity relative to the gaseous phase, each variable being represented by its time average in this statistically stationary configuration on the left, and by an instantaneous value taken at $t = 0.41$ s on the right. The profiles corresponding to the case without coalescence are also plotted. The chosen configuration is particularly interesting since the large mass oscillations of the injected spray result in a strong coupling with the dynamics and coalescence phenomena and leads to a completely different behavior as far as the dynamics and the size distributions are concerned.

Finally, the complexity of the chosen configurations, as well as the strong couplings they generate, justifies the fact that we have chosen to conduct the comparison on such test-cases.

5.4. Eulerian solvers

Two different solvers are used depending on the stationary character or not of the configuration. Let us begin with the solver for the stationary configuration. The Eulerian multi-fluid model (3.6) and (3.7) can be rewritten and simplified in the self-similar 2D axisymmetrical configuration we are considering. The resulting set of equations can be found in [1]. Since the one-way coupled equations are resolved and since the structure of the gaseous velocity field is prescribed and stationary, we only have to solve the 1D ordinary differential system of equations in the z variable for each section. The problem is then reduced to the integration of a stiff initial value problem from the inlet where the droplets are injected until the point where 99.9% of the mass has evaporated. The integration is performed using LSODE for stiff ordinary differential equations from the ODEPACK library [39]. It is based on backward differentiation formulae (BDF) methods [40] where the space step is evaluated at each iteration, given relative and absolute error tolerances [39]. The relative tolerance, for the solutions presented in the following are taken to be 10^{-4} and the absolute tolerance are related to the initial amount of mass in the various sections, since it can vary of several orders of magnitude. Repeated calculation with smaller tolerances have proved to provide the same solutions.

In order to discretize the dynamical part of the multi-fluid system (3.6) and (3.7), that is, the left hand side of the system of conservation equations for unstationary configurations, we consider a second-order finite volume kinetic scheme introduced by Bouchut et al. [32]. Indeed, without the source term, the mass density of each section and its velocity are solution of pressureless gas dynamics equations [26,27]. Let us note ρ this mass density, and (v_r, v_θ, v_z) this velocity in cylindrical coordinates (r, θ, z), without any reference to the number of the section. In the axisymetrical configuration, v_θ is zero and under the similarity assumption, the density ρ, the axial velocity $v = v_z$ and the reduced radial velocity $u = u_r/r$, only depend on the axial coordinate z and are solution of the system:

$$\begin{cases} \partial_t \rho + 2\rho u + \partial_z(\rho v) = 0, \\ \partial_t p + 3pu + \partial_z(pv) = 0, \\ \partial_t q + 2qu + \partial_z(qv) = 0, \end{cases} \tag{5.7}$$

where $p = \rho u$ and $q = \rho v$ and where the middle terms in the left hand side of the equations come from the divergence operator in cylindrical coordinates.

Let us proceed such as in [32] in order to obtain a finite volume method with a kinetic scheme for this particular system. For the pressureless system, the Maxwellian distribution making the link between the kinetic level and the equation on the macroscopic moments can be taken as a Dirac δ function [26]. Starting at time t_n with the functions $\rho^n(z)$, $u^n(z)$ and $v^n(z)$, the functions at time $t_{n+1} = t_n + \Delta t$ can be obtained by solving the transport equation derived from the similarity assumption:

$$\begin{cases} \partial_t f - \zeta^2 \partial_\zeta f + \xi \partial_z f = 0, \\ f(z, \zeta, \xi, t_n) = f^n(z, \zeta, \xi) = M(\rho^n(z), u^n(z), v^n(z), \zeta, \xi), \end{cases} \tag{5.8}$$

where the Maxwellian M is defined for any $\rho > 0$, $(u, v, \zeta, \xi) \in \mathbb{R}^4$ by

$$M(\rho, u, v, \zeta, \xi) = \rho\delta((u, v) - (\zeta, \xi)),$$

and by projecting the obtained distributions in order to get their new moments. The transport equation has the exact solution, for $0 < t < \Delta t$:

$$f(z, \zeta, \xi, t_n + t) = f^n\left(z - \xi t, \frac{\zeta}{1 - t\zeta}, \xi\right). \tag{5.9}$$

The new moments are then obtained by projecting the exact solution

$$\begin{cases} \rho^{n+1}(z) = \int_{\mathbb{R}^2} f(z,\zeta,\xi,t_{n+1})\,\mathrm{d}\zeta\,\mathrm{d}\xi, \\ p^{n+1}(z) = \int_{\mathbb{R}^2} \zeta f(z,\zeta,\xi,t_{n+1})\,\mathrm{d}\zeta\,\mathrm{d}\xi, \\ q^{n+1}(z) = \int_{\mathbb{R}^2} \xi f(z,\zeta,\xi,t_{n+1})\,\mathrm{d}\zeta\,\mathrm{d}\xi. \end{cases} \tag{5.10}$$

In order to obtain discrete values over a mesh of constant size Δz, new averages ρ_j^{n+1}, p_j^{n+1}, q_j^{n+1}, are defined by the usual expression

$$w_j^n = \frac{1}{\Delta z}\int_{z_{j-1/2}}^{z_{j+1/2}} w(z,t_n)\,\mathrm{d}z.$$

The obtained scheme can then be written as

$$\begin{cases} \rho_j^{n+1} = \rho_j^n - 2\Delta t G_j^{(1)} - \frac{\Delta t}{\Delta z}(F_{j+1/2}^{(1)} - F_{j-1/2}^{(1)}), \\ p_j^{n+1} = p_j^n - 3\Delta t G_j^{(2)} - \frac{\Delta t}{\Delta z}(F_{j+1/2}^{(2)} - F_{j-1/2}^{(2)}), \\ q_j^{n+1} = q_j^n - 2\Delta t G_j^{(3)} - \frac{\Delta t}{\Delta z}(F_{j+1/2}^{(3)} - F_{j-1/2}^{(3)}), \end{cases} \tag{5.11}$$

where the flux terms are given by

$$F_{j+1/2} = \frac{1}{\Delta t}\int_{t_n}^{t_{n+1}} \int_{\mathbb{R}^2} \begin{pmatrix} 1 \\ \zeta \\ \xi \end{pmatrix} \xi f(z_{j+1/2},\zeta,\xi,t)\,\mathrm{d}\zeta\,\mathrm{d}\xi\,\mathrm{d}t, \tag{5.12}$$

$$G_j = \frac{1}{\Delta t \Delta z}\int_{t_n}^{t_{n+1}} \int_{z_{j-1/2}}^{z_{j+1/2}} \int_{\mathbb{R}^2} \begin{pmatrix} 1 \\ \zeta \\ \xi \end{pmatrix} \zeta f(z_{j+1/2},\zeta,\xi,t)\,\mathrm{d}\zeta\,\mathrm{d}\xi\,\mathrm{d}z\,\mathrm{d}t. \tag{5.13}$$

The obtained fluxes rely, through (5.8), on the knowledge of functions $\rho^n(z)$, $u^n(z)$ and $v^n(z)$, which have to be determined from the discrete values ρ_j^n, p_j^n and q_j^n. We use piecewise constant over half-cells, as for the simplified second-order kinetic scheme defined in [32]. If we do not write, on purpose for the sake of legibility, the n exponent, the moments take the form

$$\begin{cases} \rho(z) = \rho_{j-1/2}^R, \quad u(z) = u_{j-1/2}^R, \quad v(z) = v_{j-1/2}^R, \quad z_{j-1/2} < z < z_j, \\ \rho(z) = \rho_{j+1/2}^L, \quad u(z) = u_{j+1/2}^L, \quad v(z) = v_{j+1/2}^L, \quad z_j < z < z_{j+1/2}, \end{cases} \tag{5.14}$$

with

$$\begin{cases} \rho_{j+1/2}^L = \rho_j + D\rho_j \Delta z/2, & \rho_{j+1/2}^R = \rho_{j+1} - D\rho_{j+1}\Delta z/2, \\ u_{j+1/2}^L = \bar{u}_j + Du_j \Delta z/2, & u_{j+1/2}^R = \bar{u}_{j+1} - Du_{j+1}\Delta z/2, \\ v_{j+1/2}^L = \bar{v}_j + Dv_j \Delta z/2, & v_{j+1/2}^R = \bar{v}_{j+1} - Dv_{j+1}\Delta z/2. \end{cases} \tag{5.15}$$

In order to satisfy the momentum conservation, $\bar{u}_j$ and $\bar{v}_j$ are chosen as

$$\bar{u}_j = u_j - \frac{D\rho_j Du_j}{4\rho_j}\Delta z^2, \quad \bar{v}_j = v_j - \frac{D\rho_j Dv_j}{4\rho_j}\Delta z^2,$$

with $u_j = p_j/\rho_j$ and $v_j = q_j/\rho_j$.

The CFL conditions is defined for this explicit scheme as

$$\Delta t \sup_z |u^n(z)| \leqslant \Delta z/2, \quad \Delta t \sup_z |v^n(z)| \leqslant \Delta z/2,$$

and the obtained scheme reads

$$F_{j+1/2} = \frac{\rho^L_{j+1/2} v^L_{j+1/2}}{1 + u^L_{j+1/2}\Delta t} \begin{pmatrix} u^L_{j+1/2} & \dfrac{1 + u^L_{j+1/2}\Delta t/2}{1 + u^L_{j+1/2}\Delta t} \\ & v^L_{j+1/2} \end{pmatrix}, \tag{5.16}$$

and

$$\begin{aligned} G_j = {} & \frac{\Delta t \rho^L_{j-1/2} v^L_{j-1/2} u^L_{j-1/2}}{2\Delta z (1 + u^L_{j-1/2}\Delta t)^2} \begin{pmatrix} u^L_{j-1/2} & \dfrac{1 + u^L_{j-1/2}\Delta t/3}{1 + u^L_{j-1/2}\Delta t} \\ & v^L_{j-1/2} \end{pmatrix} \\ & + \frac{\rho^R_{j-1/2} u^R_{j-1/2}}{2(1 + u^R_{j-1/2}\Delta t)^2} \begin{pmatrix} & 1 + u^R_{j-1/2}\dfrac{\Delta t}{2} \\ u^R_{j-1/2} & \dfrac{1 + u^R_{j-1/2}\Delta t + (u^R_{j-1/2})^2 \Delta t^2/3}{1 + u^R_{j-1/2}\Delta t} \\ & v^R_{j-1/2}\left(1 + u^R_{j-1/2}\dfrac{\Delta t}{2}\right) \end{pmatrix} \\ & + \frac{\rho^L_{j+1/2} u^L_{j+1/2}}{2(1 + u^L_{j+1/2}\Delta t)^2} \begin{pmatrix} & 1 - \dfrac{\Delta t}{\Delta z} v^L_{j+1/2} + u^L_{j+1/2}\dfrac{\Delta t}{2} \\ u^L_{j+1/2} & \dfrac{1 + u^L_{j+1/2}\Delta t + (u^L_{j+1/2})^2 \Delta t^2/3 - \dfrac{\Delta t}{\Delta z} v^L_{j+1/2}(1 + u^L_{j+1/2}\Delta t/3)}{1 + u^L_{j+1/2}\Delta t} \\ & v^L_{j+1/2}\left(1 - \dfrac{\Delta t}{\Delta z} v^L_{j+1/2} + u^L_{j+1/2}\dfrac{\Delta t}{2}\right) \end{pmatrix}. \end{aligned} \tag{5.17}$$

The vaporization, coalescence and drag forces source terms are then added in order to perform the simulations.

The reduced CPU times for both the monomodal and bimodal distributions are presented in Table 2 in the stationary configuration and in Table 3, for the unstationary one. It is worth noticing that the complexity behaves like the number of sections to the square, but more importantly, that the resolution of the coalescence phenomenon only brings in an additional cost of about 50% compared to the computation without the coalescence quadratic terms.

5.5. The stationary case

The Eulerian multi-fluid model is especially well-suited for the monomodal distribution where a large and continuous spectrum of droplets is present, with a distribution tail. It can be seen in Fig. 10-left, that

Table 2
Reduced CPU time for the stationary configuration

No. sections	Mon. without collision	Mon. with collision	No. sections	Bim. without collision	Bim. with collision
90	22.7	35.2	100	70.9	114.1
60	10.9	25.6	50	16.0	24.0
30	3.0	4.2	25	9.0	13.0
15	1.0	1.8	13	1.0	1.3

Table 3
Reduced CPU time for the unstationary configuration and second size distribution

No. sections	Unstationary without collision	Unstationary with collision
90	22.0	35.0
30	3.1	4.7
15	1.0	1.4

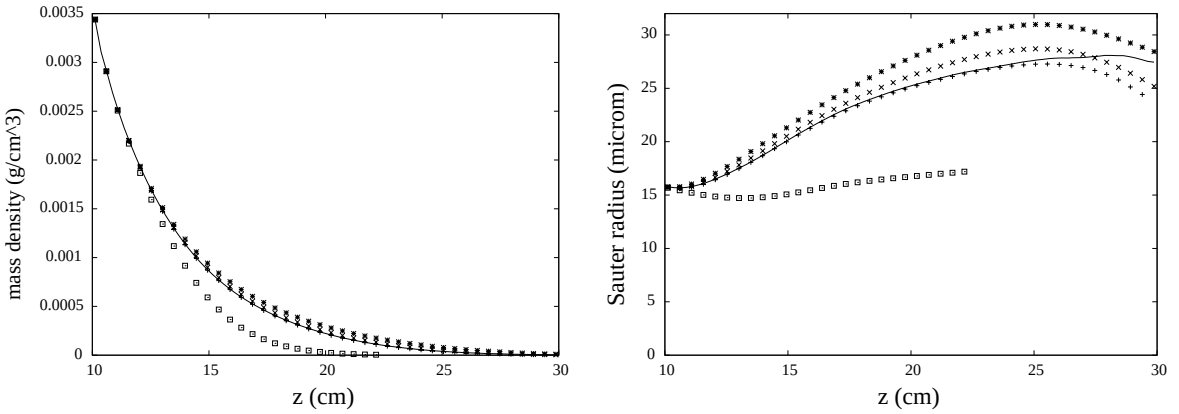

Fig. 10. (left) Evolution of the mass density of liquid for the Lagrangian reference solution (solid line) and for various discretizations with the Eulerian multi-fluid model (+: 90 sections, ×: 30 section, *: 15 sections, □: 90 sections without collision). (right) Sauter mean radius for the Lagrangian reference solution (solid line) and for various discretizations with the Eulerian multi-fluid model (+: 90 sections, ×: 30 section, *: 15 sections, □: 90 sections without collision).

the curves corresponding to the 90 sections solutions and the reference Lagrangian solution almost coincide; the difference never gets bigger that five per a thousand of the initial mass density of droplets. This, on the one side, demonstrates the ability of the Eulerian model to simulate the proposed configuration, and on the other hand provides a numerical validation tool for the Lagrangian solver.

As mentioned previously, the strength of such multi-fluid models, is to be able to reproduce the global behavior of the spray with a limited number of sections. Consequently, calculations with various numbers of sections were performed: 90, 60, 30 and 15. For completeness, we have also represented, both in Fig. 10 left and right, the solution without coalescence calculated with 90 sections (which is superimposed on the one calculated with the reference Lagrangian solver in Fig. 10-left). The conclusion to be drawn from these figures is that the multi-fluid is able to predict fairly well, even in the case of 15 sections for which the computational cost is very reasonable, the global coupling of the various phenomena occurring in the nozzle. One crucial point is related to the localization of the evaporation front for pollutant formation purposes and even with 15 sections, the evaporation front is precisely computed.

It is particularly interesting to note that the average dynamics are correctly reproduced with 90 sections. Concerning the Sauter mean radius of the distribution, it is extremely well-predicted by the 90 section solution, fairly well-reproduced by the 30 section one and the difference gets bigger when we use 15 sections, even if the mass difference does not get bigger than 2% of the initial one.

If the monomodal distribution is well suited for the Eulerian multi-fluid approach, the bimodal one can be considered as the most difficult task; first the method can be shown to be of first-order in the size discretization step [28] and some previous calculations have proved the difficulty of calculating the

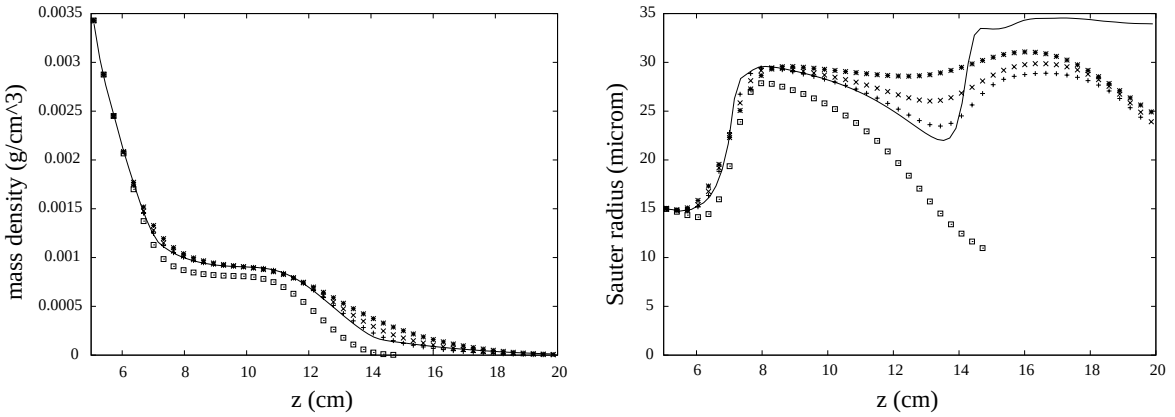

Fig. 11. (left) Evolution of the mass density of liquid for the Lagrangian reference solution (solid line) and for various discretizations with the Eulerian multi-fluid model (+: 100 sections, ×: 50 section, *: 25 sections, □: 100 sections without collision). (right) Sauter mean radius for the Lagrangian reference solution (solid line) and for various discretizations with the Eulerian multi-fluid model (+: 100 sections, ×: 50 section, *: 25 sections, □: 100 sections without collision).

interaction of two groups like the one proposed in this example [8]. In such a situation, the numerical diffusion is introducing some artificial coupling at the dynamical level since only one velocity is prescribed per section.

However, the results presented in Fig. 11 show that the mass evolution is very well captured, the difference with the reference solution stays below 1%. The evolution of the Sauter mean radius in Fig. 11-right is also well captured. However, once 93% of the initial mass has evaporated, there is a little difference in the mass density decrease which seems to be due to a difficulty to correctly reproduce the dynamics and size distribution of the spray.

In order to have a more precise idea of what is happening, we have observed the mass distribution function at the point $z = 10.53$ cm as well as the velocity distribution as a function of the droplet size at this point. It appears very clearly that the numerical diffusion, if too high, can smooth out the mass distribution function and consequently the velocity distribution function because of the assumption, the Eulerian multi-fluid model relies on. In the 25 sections case, the peaks of the distribution have disappeared and the velocity distribution function has become monotone. This example allows to understand what will be the limits of such an approach. However, the simulation with 100 sections allows to predict very accurately the various peaks of the mass distribution function, as well as their dynamics, except for the very "big" droplets, the velocity of which is becoming higher thus causing the difference to be observed in Fig. 11-right on the Sauter mean radius. This discrepancy can be attributed to the numerical diffusion [28] which acts on a size distribution function which is very singular and remains so through the coalescence phenomenon. The smearing out of the peaked distribution is then coupled to the dynamics and coalescence phenomena; it thus leads to a change in the Sauter mean diameter as observed in Fig. 11-right.

5.6. The unstationary case

In the same way as for the Lagrangian calculations, we have represented in Figs. 12–14, the averaged quantities for this statistically stationary configuration as well as the instantaneous fields of mass density, mean velocity and Sauter mean radius at a given time $t = 0.41$ s. The simulations conducted with the Eulerian multi-fluid model with three level of refinement, 15, 30 and 90 sections, are compared to the "reference" Lagrangian solution.

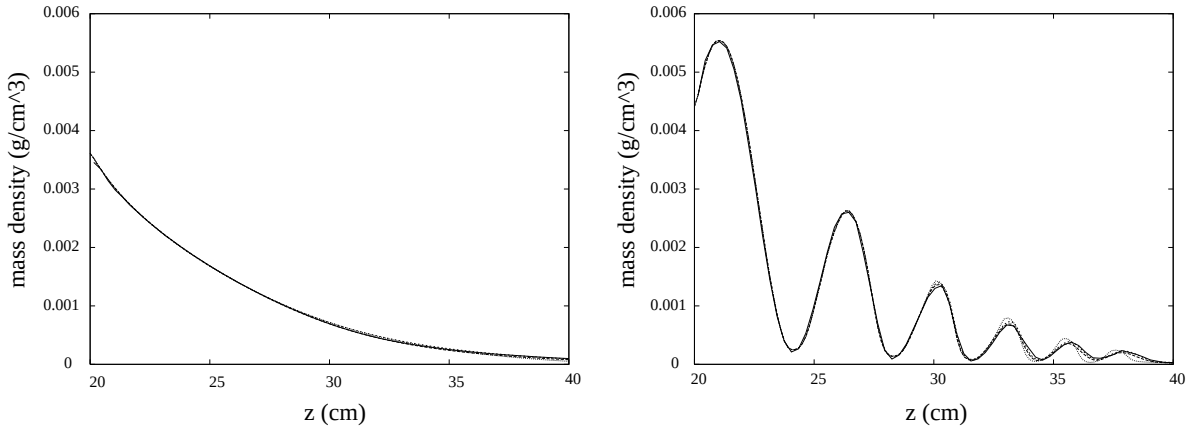

Fig. 12. (left) Evolution of the temporal averaging of the liquid mass density for the Lagrangian reference solution (solid line), and for various discretizations with the Eulerian multi-fluid model (dashed line: 90 sections; dotted line: 30 section; small dotted line: 15 sections), for the unstationary case with collisions, (right) evolution of the mass density of the liquid at $t = 0.41$ s for the Lagrangian reference solutions (solid line), and for various discretizations with the Eulerian multi-fluid model (dashed line: 90 sections; dotted line: 30 section; small dotted line: 15 sections), for the unstationary case with collisions.

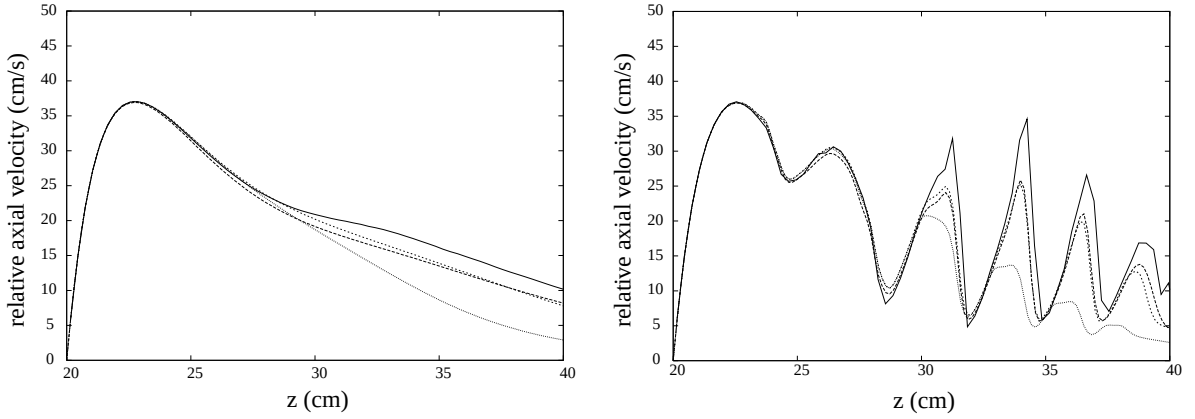

Fig. 13. (left) Evolution of the temporal averaging of the axial mean velocity difference of the liquid for the Lagrangian reference solution (solid line), and for various discretizations with the Eulerian multi-fluid model (dashed line: 90 sections; dotted line: 30 section; small dotted line: 15 sections), for the unstationary case with collisions, (right) Evolution of the axial mean velocity difference of the liquid at $t = 0.41$ s for the Lagrangian reference solutions (solid line), and for various discretizations with the Eulerian multi-fluid model (dashed line: 90 sections; dotted line: 30 section; small dotted line: 15 sections), for the unstationary case with collisions.

The chosen configuration is particularly interesting. The averaged mass as well as the instantaneous spatial profile of mass density are well predicted by the three discretizations, even if one can observe a shift in the oscillations starting around 33 cm for the discretization with 15 sections. Because of the coupling between the dynamics of droplets of various sizes and the coalescence, the spray mean velocity profile, which is the one of the gas at the injection, as well as the Sauter mean diameter, experiences strong oscillations.

At this level, considering the complexity of the behavior of the size distribution of droplets, the discretization with 15 sections is not able to reproduce precisely the global dynamical behavior of the spray

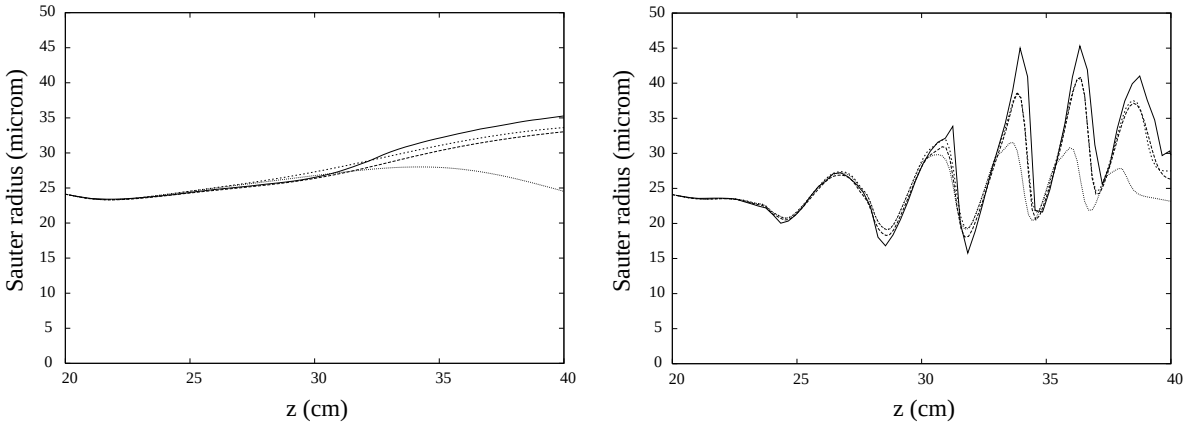

Fig. 14. (left) Evolution of the temporal averaging of the liquid Sauter mean radius for the Lagrangian reference solution (solid line), and for various discretizations with the Eulerian multi-fluid model (dashed line: 90 sections; dotted line: 30 section; small dotted line: 15 sections), for the unstationary case with collisions, (right) evolution of the Sauter mean radius of the liquid at $t = 0.41$ s for the Lagrangian reference solutions (solid line), and for various discretizations with the Eulerian multi-fluid model (dashed line: 90 sections; dotted line: 30 section; small dotted line: 15 sections), for the unstationary case with collisions.

beyond $z = 30$ cm, as represented in Fig. 13-left. The reason is the same as in the stationary bimodal case: the numerical diffusion for this coarse discretization acting on a discontinuous size distribution function is little by little coupled to the coalescence and size-conditioned dynamics. It results first in a damping of the velocity and Sauter mean radius oscillations, and soon in a shift of these oscillations compared to the reference solution. However, the discretizations with 30 and 90 sections lead to a satisfactory comparison with this reference solution, even if the numerical diffusion still acts on the discontinuous size distribution function and results in small discrepancies.

5.7. The zero dispersion assumption and the computational efficiency

In order to have a comprehensive picture for the discussion about the comparison of the Lagrangian and Eulerian approaches, we still need to investigate two points. The first one is related to the fundamental assumption on the velocity dispersion which allows the derivation of the semi-kinetic model and the second one is related to the compared computational efficiency of these methods.

It is clear that the coalescence phenomenon is going to induce a velocity dispersion around the mean value of the velocity. Let us first consider the stationary case with the monomodal distribution. We have plotted, in Fig. 15, the velocity marginals for each droplet size at a given spatial point $z = 16.6$ cm. Whereas the small droplets have almost zero dispersion, it can reach 3% of the local mean velocity for the droplets of radius around 40 μm. We have chosen this point because it is one of the points where this dispersion reaches its maximum value as shown in Fig. 16-top where the variance of the dispersion relative to the local velocity is presented as a function of spatial coordinate and droplet size. There are only three points where it goes beyond 1.2% and reaches 3%, so that the vertical scale has been limited to 1.2% in order to describe the global behavior if this dispersion. The same scale is chosen for the bimodal case represented in Fig. 16-bottom without excluding any point. At the entrance of the nozzle, the dispersion is almost zero and it increases for the droplets created by coalescence. However, because of the evaporation process and of the drag force, the Stokes relaxation time of which is linear in the droplet surface, the size of the droplets decreases with time and there velocity relaxes to the one on the gas thus limiting the velocity dispersion

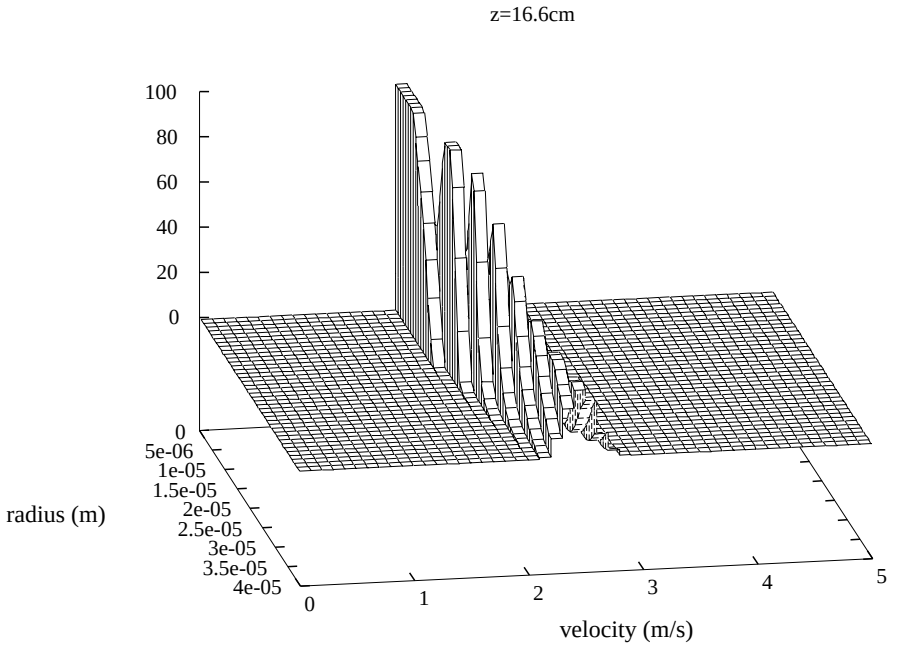

Fig. 15. Velocity marginals, for each droplet size, at $z = 16.6$ cm, for the monomodal case with coalescence.

(Fig. 16). The presence of this dispersion is also related to the fact that the nozzle for the stationary cases has been chosen such that the deceleration is very important.

For the unstationary case, where the deceleration is take at a little lower value, the dispersion stays below 2 per thousand. We have plotted in Fig. 17 the velocity marginals as a function of size at two locations $z = 31.5$ cm and $z = 27$ cm at time $t = 0.41$ s. It is clear that the dispersion is very limited.

Consequently, the assumption that there exists one characteristic velocity around which there is no dispersion for a given time, a given location and a given size can be considered, at least in the test-cases we have considered, as very realistic. If one would want to be able to tackle even more severe cases with much bigger droplets for example, the dispersion would probably become larger and one would have to introduce a ''temperature'' for each ''fluid'', as we have proposed in the turbulent case in [25].

The second point, which is important, is the computational efficiency of the Eulerian multi-fluid model as compared to the Lagrangian one. Before going into the numbers, let us underline that such results can only provide an indication since the structure of the two codes are completely different and since we only consider here the solver for the liquid phase, whereas a major advantage of the Eulerian approach is that it leads to the capability of optimizing the two coupled Eulerian solvers for the gas and the liquid phase. Nevertheless, on a recent PC workstation, the simulation of the injection of the spray in an empty nozzle at $t = 0$ until $t = .41$ s with the beginning of the mass oscillations at the injection point at $t = .332$ s takes 3.4 min with Eulerian approach with 15 sections, 11.8 with 30 sections and 87 with 90 sections, whereas it takes 2.8 min for the case Lag. Unst. 1, 40 for the second one and 213 for the third one. Consequently, for a reasonable level of precision reached for example by the intermediate simulations with both solvers, the Eulerian one is comparable but a little cheaper. Even if we understand the limits of such a comparison, it shows that the Eulerian multi-fluid model is going to be able to reach a very reasonable level of precision for a computational cost which is lower but comparable to the Lagrangian approach; however it is going to allow optimization of coupled Eulerian solvers for the gas and the liquid and to avoid, in higher-dimensional

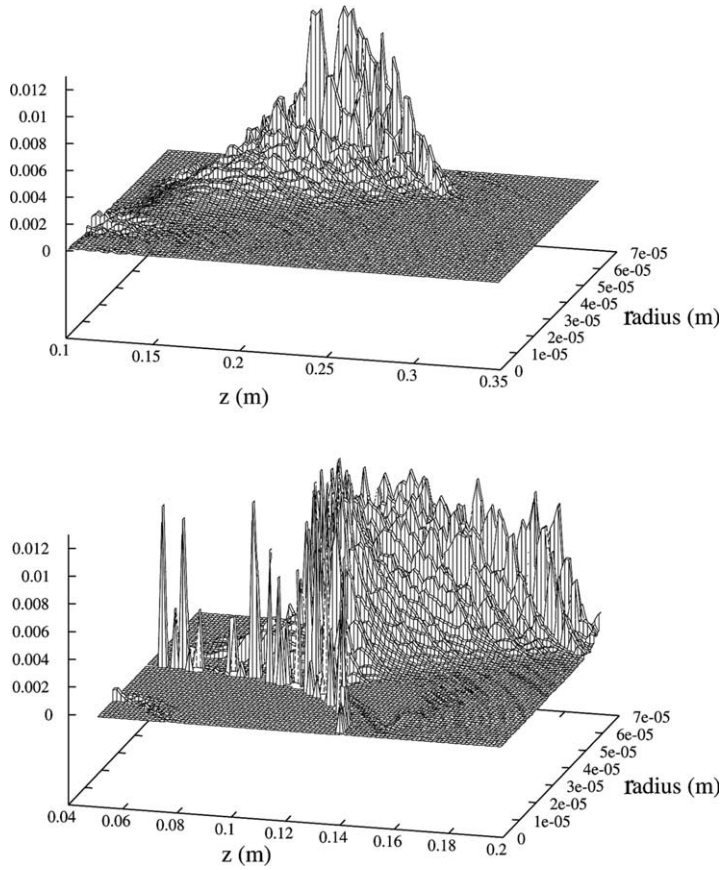

Fig. 16. (top) Evolution of the velocity dispersion compared to the square of the mean velocity for each droplet size, for the monomodal case with coalescence, (bottom) evolution of the velocity dispersion compared to the square of the mean velocity for each droplet size, for the bimodal case with coalescence.

configuration, the problem of small numbers of particles in computational cell, a crucial problem in combustion applications.

6. Discussion and conclusion

We have proposed a new Eulerian multi-fluid approach in order to simulate polydisperse evaporating dense sprays. This approach can be rigorously derived from the Williams p.d.f. equation at the kinetic level and allows for a description of the droplet coalescence phenomenon, an uncommon feature of the usual Eulerian models. The main advantage of such an approach, which can be thought of as intermediate between discrete particle Lagrangian solvers and two-fluid models, is that it provides an adaptable level of information about the size distribution depending on the problem to be solved.

We have proved the ability of such a method to reproduce the solution provided by a reference Lagrangian solver in the configuration of a 2D axisymmetrical nozzle configuration with both stationary and unstationary test-cases. These test-cases have been described and explained to be complex enough configurations, since the problem is essentially unstationary, 2D in space (reduced to 1D by similarity) and 1D

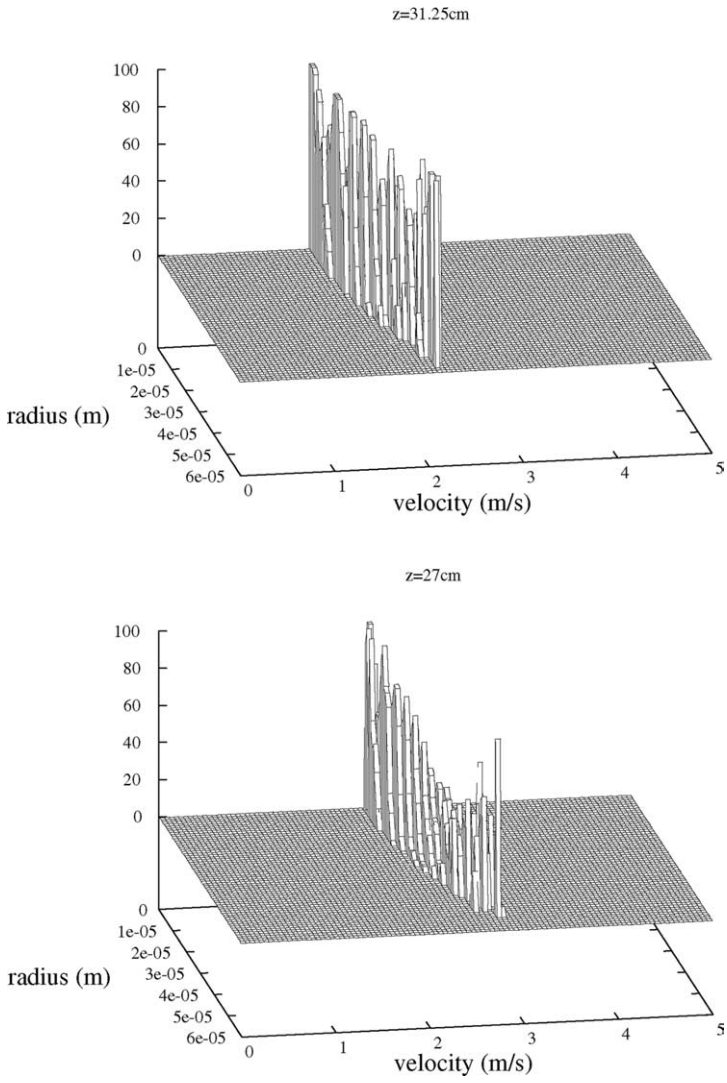

Fig. 17. (top) Velocity marginals, for each droplet size, at $z = 31.25$ cm, for the unstationary case with coalescence, (bottom) velocity marginals, for each droplet size, at $z = 27.00$ cm, for the unstationary case with coalescence.

in size phase space and involves strong couplings between evaporation, dynamics and coalescence. The limitations of the approach have been presented as well as its strength. In particular, the assumptions underlying the model have been shown to be very reasonable by considering the reference solution and the question of zero velocity dispersion at a given time, given space location and droplet size has been addressed and shown to be a good approximation.

The Eulerian multi-fluid model is able to reproduce the global qualitative behavior of the spray with a very limited number of unknowns at a very low computational cost. In such a case, where a particulate Lagrangian solver produces artificial fluctuations due to the limited number of particles for a comparable computational cost, the Eulerian solver smoothens out the fluctuations artificially and does not yield precise solutions. In order to be quantitative, the size discretization necessary to approximate the reference

Lagrangian solution obtained with a very large number of particles leads to a reasonable computational cost as compared with the same level of precision for the Lagrangian solver. However, the numerical diffusion in the size phase space in order to describe the evaporation phenomenon results in a difficulty to deal with singular size distributions like discontinuous or Dirac delta functions. In such a situation, it introduces artificial small couplings and smoothens out the details of the fluctuations of the dynamics of the droplets. This can be related to the only first-order in the size variable of the approach as studied in [28]. However, it yields a computational tool, complementary to the class of Lagrangian solvers, which is able, for the first time, to describe the details of the size distributions of a spray constituted of droplets having their own inertia, in a Eulerian way.

In a recent work, the premises of which are presented in [22,24,28], we have introduced a new high order method for the evaporation which can be extended to dense sprays with coalescence. This will allow to further reduce the number of sections thus reinforcing the efficiency of the tool we have developed for more complex configurations and leading to a new class of refined Eulerian solvers as compared to the ones of two-fluid type.

Acknowledgements

We would like to thank R.O. Fox for several helpful discussions.

Appendix A

The purpose of this Appendix is to restore the details of the proof of Proposition 3.1 of Section 3.1. We have seen that the assumption of zero dispersion is not compatible with the coalescence term and the conservation of momentum. Starting from assumptions [H1] and [H3], we then consider a small and uniform dispersion σ which is going to converge to zero and make the following assumption instead of [H2]:

[D1] At a given size, the velocity distribution in each space direction, $k = 1, K$, is a Gaussian function φ_σ of dispersion σ around $\overline{u}_k(t,x,v)$:

$$f(t,x,v,u) = n(t,x,v)\prod_{k=1}^{K}\varphi_\sigma(u_k - \overline{u}_k(t,x,v)). \tag{A.1}$$

Let us notice that [D1] implies [H1]. We then use the same arguments as in [8] in order to obtain the macroscopic conservation equations when coalescence is present through the collisional operator Γ. The transport Eq. (2.1) is multiplied by 1 and u; we then integrate with respect to the velocity variable. We then obtain a first set of conservation equations parametrized by the size of the droplets:

$$\begin{aligned}\partial_t n + \partial_x\cdot(n\overline{u}) + \partial_v(nR_v) = & -n(v)\int_{v^*} n(v^*)\beta(v,v^*)I_n^-\,\mathrm{d}v^* \\ & + \frac{1}{2}\int_{v^*\in[0,v]} n(v^\diamondsuit(v,v^*))n(v^*)\beta(v^\diamondsuit(v,v^*),v^*)I_n^+\,\mathrm{d}v^*,\end{aligned} \tag{A.2}$$

$$\begin{aligned}\partial_t(n\overline{u}) + \partial_x\cdot(n\overline{u}\otimes\overline{u} + n\boldsymbol{P}(\sigma)) + \partial_v(nR_v\overline{u}) - n\overline{F} = & -n(v)\int_{v^*} n(v^*)\beta(v,v^*)I_u^-\,\mathrm{d}v^* \\ & + \frac{1}{2}\int_{v^*\in[0,v]} n(v^\diamondsuit(v,v^*))n(v^*)\beta(v^\diamondsuit(v,v^*),v^*)I_u^+\,\mathrm{d}v^*,\end{aligned} \tag{A.3}$$

where $\overline{F}$ is the Stokes's drag force taken at $u = \overline{u}$ and where the partial collisional integrals I_n^-, I_n^+, I_u^- and I_u^+ take the following expressions:

$$I_n^-(v, v^*, \sigma) = \int_{u,u^*} \int |u - u^*| \varphi_\sigma(u - \overline{u}(v)) \varphi_\sigma(u^* - \overline{u}(v^*)) \, \mathrm{d}u \, \mathrm{d}u^*, \tag{A.4}$$

$$I_u^-(v, v^*, \sigma) = \int_{u,u^*} \int u|u - u^*| \varphi_\sigma(u - \overline{u}(v)) \varphi_\sigma(u^* - \overline{u}(v^*)) \, \mathrm{d}u \, \mathrm{d}u^*, \tag{A.5}$$

$$I_n^+(v, v^*, \sigma) = \int_{u^\diamondsuit,u^*} \int |u^\diamondsuit - u^*| \varphi_\sigma(u^* - \overline{u}(v^*)) \varphi_\sigma(u^\diamondsuit - \overline{u}(v - v^*)) \, \mathrm{d}u^\diamondsuit \, \mathrm{d}u^*, \tag{A.6}$$

$$vI_u^+(v, v^*, \sigma) = \int_{u^\diamondsuit,u^*} \int \big((v - v^*)u^\diamondsuit + v^* u^*\big) |u^\diamondsuit - u^*| \varphi_\sigma(u^* - \overline{u}(v^*)) \varphi_\sigma(u^\diamondsuit - \overline{u}(v - v^*)) \, \mathrm{d}u^\diamondsuit \, \mathrm{d}u^*. \tag{A.7}$$

In the previous expressions, we have used the new velocity variables $(u^\diamondsuit, u^*)$ in the creation integrals. It is here fundamental that assumptions [D1] and [H3] are satisfied, i.e. that the support of the distributions in size and velocities is really the whole space $(v, u) \in (0, +\infty) \times \mathbb{R}^K$ so that all the collisions can be described by our model.

Lemma 8.1. *When the dispersion σ goes to zero, we have the following convergence:*

$$\boldsymbol{P} \to \boldsymbol{O}_{\boldsymbol{K}\times\boldsymbol{K}}, \quad I_n^- \to |\overline{u}(v) - \overline{u}(v^*)|, \quad I_u^- \to \overline{u}(v)|\overline{u}(v) - \overline{u}(v^*)|, \tag{A.8}$$

$$I_n^+ \to |\overline{u}(v^*) - \overline{u}(v - v^*)|, \quad vI_u^+ \to ((v - v^*)\overline{u}(v - v^*) + v^*\overline{u}(v^*))|\overline{u}(v^*) - \overline{u}(v - v^*)|. \tag{A.9}$$

Proof. It can be easily proved that, up to an error linear in the dispersion σ, it is sufficient to consider the 1D case. We then switch to the polar coordinates around the point $(\overline{u}(v), \overline{u}(v^*))$ with $\Psi = \overline{u}(v) - \overline{u}(v^*)$.

$$I_n^- = \int_{r,\theta} \int \frac{r \exp(-r^2/\sigma^2)}{\sigma^2} |r(cos(\theta) - sin(\theta)) + \Psi| \, \mathrm{d}r \, \mathrm{d}\theta.$$

Two cases are then to be distinguished, either $\Psi = 0$ and $I_n^- = \sqrt{2\pi}\sigma$, either $\Psi \neq 0$ and $I_n^- - \Psi \to 0$ when σ becomes lower than the distance between Ψ and 0 so that the Gaussian distribution approaches a Dirac delta function.

$$I_n^- - \Psi = \int_{r,\theta} \int \frac{r \exp(-r^2/\sigma^2)}{\pi\sigma^2} (|r(cos(\theta) - sin(\theta)) - \Psi| - \Psi) \, \mathrm{d}\theta.$$

For all given ε and Ψ, there exists a small disk D of radius δ around zero such that on D, $|r(\cos(\theta) - \sin(\theta)) - \Psi| - \Psi \leqslant \varepsilon/2$ and there exists σ such that on the complementary of D, the previous integral is lower than $\varepsilon/2$; consequently, $I_n^- - \Psi \to 0$ as $\sigma \to 0$. The other integrals are treated following the same arguments. □

Finally if we pass to the limit of zero dispersion in Eqs. (A.2) and (A.3), we obtain the semi-kinetic model presented in Section 3.1 by Eqs. (3.1) and (3.2) and the proof is complete.

Appendix B

The purpose of the present Appendix is to restore the details of the evaluation of the quadratic coalescence terms in the conservation Eqs. (3.6)–(3.9) from the semi-kinetic model (3.1) and (3.2).

Let us come back to the definition of the coalescence terms in (3.6) and (3.7):

$$\begin{aligned} C_{\mathrm{m}}^{(j)} = & -\sum_{k=1}^{N} m^{(k)} \int_{v^{(j)}}^{v^{(j+1)}} \rho_l v^* f(v^*) \int_{v^{(k-1)}}^{v^{(k)}} f(v) B(\overline{u}^{(j)} - \overline{u}^{(k)}, v, v^*)\, \mathrm{d}v^*\, \mathrm{d}v \\ & + \frac{1}{2} \iint_{D_j^{\diamondsuit *}} \rho_l n(v^\diamondsuit) n(v^*)(v^\diamondsuit + v^*) B(\overline{u}(v^*) - \overline{u}(v^\diamondsuit), v^*, v^\diamondsuit)\, \mathrm{d}v^*\, \mathrm{d}v^\diamondsuit, \end{aligned} \tag{B.1}$$

$$\begin{aligned} C_{\mathrm{mu}}^{(j)} = & -m^{(j)} \overline{u}^{(j)} \sum_{k=1}^{N} m^{(k)} \int_{v^{(j-1)}}^{v^{(j)}} \rho_l v^* f(v^*) \int_{v^{(k-1)}}^{v^{(k)}} f(v) B(\overline{u}^{(j)} - \overline{u}^{(k)}, v, v^*)\, \mathrm{d}v^*\, \mathrm{d}v \\ & + \frac{1}{2} \iint_{D_j^{\diamondsuit *}} \rho_l n(v^\diamondsuit) n(v^*)(v^\diamondsuit \overline{u}(v^\diamondsuit) + v^* \overline{u}(v^*)) B(\overline{u}(v^*) - \overline{u}(v^\diamondsuit), v^*, v^\diamondsuit)\mathrm{d}v^*\, \mathrm{d}v^\diamondsuit. \end{aligned} \tag{B.2}$$

At this level, we make assumption (3.5) on n and f in such a way that we introduce the mass densities in the sections $m^{(j)}$. Besides, we take advantage of the fact that the velocity is constant inside a section, so that the right integration supports are introduced:

$$\begin{aligned} C_{\mathrm{m}}^{(j)} = & -m^{(j)} \sum_{k=1}^{N} m^{(k)} V_{jk} \iint_{L_{jk}} \rho_l v \kappa^{(j)}(v) \kappa^{(k)}(v^*) \beta(v, v^*)\, \mathrm{d}v\, \mathrm{d}v^* \\ & + \frac{1}{2} \sum_{i=1}^{I^{(j)}} m^{(o_{ji}^\diamondsuit)} m^{(o_{ji}^*)} V_{o_{ji}^\diamondsuit o_{ji}^*} \left(\iint_{X_{ji}} \rho_l v^\diamondsuit \kappa^{(o_{ji}^\diamondsuit)}(v^\diamondsuit) \kappa^{(o_{ji}^*)}(v^*) \beta(v^\diamondsuit, v^*)\, \mathrm{d}v^*\, \mathrm{d}v^\diamondsuit \right. \\ & + \iint_{X_{ji}} \rho_l v^* \kappa^{(o_{ji}^\diamondsuit)}(v^\diamondsuit) \kappa^{(o_{ji}^*)}(v^*) \beta(v^\diamondsuit, v^*)\, \mathrm{d}v^*\, \mathrm{d}v^\diamondsuit \\ & + \iint_{X_{ji}^{\mathrm{sym}}} \rho_l v^\diamondsuit \kappa^{(o_{ji}^*)}(v^\diamondsuit) \kappa^{(o_{ji}^\diamondsuit)}(v^*) \beta(v^\diamondsuit, v^*)\, \mathrm{d}v^*\, \mathrm{d}v^\diamondsuit \\ & \left. + \iint_{X_{ji}^{\mathrm{sym}}} \rho_l v^* \kappa^{(o_{ji}^*)}(v^\diamondsuit) \kappa^{(o_{ji}^\diamondsuit)}(v^*) \beta(v^\diamondsuit, v^*)\, \mathrm{d}v^*\, \mathrm{d}v^\diamondsuit \right), \end{aligned} \tag{B.3}$$

$$
\begin{aligned}
C_{\mathrm{mu}}^{(j)} = & -m^{(j)}\overline{u}^{(j)}\sum_{k=1}^{N} m^{(k)} V_{jk}\int\int_{L_{jk}} \rho_l v \kappa^{(j)}(v)\kappa^{(k)}(v^*)\beta(v,v^*)\,\mathrm{d}v\,\mathrm{d}v^* \\
& + \frac{1}{2}\sum_{i=1}^{I^{(j)}} m^{(o_{ji}^{\diamondsuit})} m^{(o_{ji}^{*})} V_{o_{ji}^{\diamondsuit} o_{ji}^{*}} \Bigg(\overline{u}^{(o_{ji}^{\diamondsuit})} \int\int_{X_{ji}} \rho_l v^{\diamondsuit} \kappa^{(o_{ji}^{\diamondsuit})}(v^{\diamondsuit})\kappa^{(o_{ji}^{*})}(v^*)\beta(v^{\diamondsuit},v^*)\,\mathrm{d}v^*\mathrm{d}v^{\diamondsuit} \\
& + \overline{u}^{(o_{ji}^{*})} \int\int_{X_{ji}} \rho_l v^* \kappa^{(o_{ji}^{\diamondsuit})}(v^{\diamondsuit})\kappa^{(o_{ji}^{*})}(v^*)\beta(v^{\diamondsuit},v^*)\,\mathrm{d}v^*\,\mathrm{d}v^{\diamondsuit} \\
& + \overline{u}^{(o_{ji}^{*})} \int\int_{X_{ji}^{\mathrm{sym}}} \rho_l v^{\diamondsuit} \kappa^{(o_{ji}^{*})}(v^{\diamondsuit})\kappa^{(o_{ji}^{\diamondsuit})}(v^*)\beta(v^{\diamondsuit},v^*)\,\mathrm{d}v^*\,\mathrm{d}v^{\diamondsuit} \\
& + \overline{u}^{(o_{ji}^{\diamondsuit})} \int\int_{X_{ji}^{\mathrm{sym}}} \rho_l v^* \kappa^{(o_{ji}^{*})}(v^{\diamondsuit})\kappa^{(o_{ji}^{\diamondsuit})}(v^*)\beta(v^{\diamondsuit},v^*)\,\mathrm{d}v^*\,\mathrm{d}v^{\diamondsuit} \Bigg).
\end{aligned} \tag{B.4}
$$

This yields the final system of equations and we recall the expression of the collisional integrals:

$$
\mathcal{Q}_{jk} = \int\int_{L_{jk}} \rho_l v \kappa^{(j)}(v)\kappa^{(k)}(v^*)\beta(v,v^*)\,\mathrm{d}v\,\mathrm{d}v^*, \quad \mathcal{Q}_{ji}^{\diamondsuit} = \int\int_{X_{ji}} \rho_l v^{\diamondsuit} \kappa^{(o_{ji}^{\diamondsuit})}(v^{\diamondsuit})\kappa^{(o_{ji}^{*})}(v^*)\beta(v^{\diamondsuit},v^*)\,\mathrm{d}v^*\,\mathrm{d}v^{\diamondsuit},
$$

$$
\mathcal{Q}_{ji}^{*} = \int\int_{X_{ji}} \rho_l v^* \kappa^{(o_{ji}^{\diamondsuit})}(v^{\diamondsuit})\kappa^{(o_{ji}^{*})}(v^*)\beta(v^{\diamondsuit},v^*)\,\mathrm{d}v^*\,\mathrm{d}v^{\diamondsuit} = \int\int_{X_{ji}^{\mathrm{sym}}} \rho_l v^{\diamondsuit} \kappa^{(o_{ji}^{*})}(v^{\diamondsuit})\kappa^{(o_{ji}^{\diamondsuit})}(v^*)\beta(v^{\diamondsuit},v^*)\,\mathrm{d}v^*\mathrm{d}v^{\diamondsuit}.
$$

We have represented the strip $D_4^{\diamondsuit *}$, X_{4i}, $i = 1,4$ and X_{4i}^{sym}, $i = 1,2$ in Fig. 1, as well as the rectangular integration domains L_{42} and L_{24} for the disappearance operator. Let us recall

$$
D_j^{\diamondsuit *} = \bigcup_{k=2}^{N}\bigcup_{l=1}^{k-1}\left(L_{kl}\cap D_j^{\diamondsuit *}\right)\cup\left(L_{lk}\cap D_j^{\diamondsuit *}\right) = \bigcup_{i=1}^{I^{(j)}}\left(X_{ji}\cup X_{ji}^{\mathrm{sym}}\right), X_{ji} = L_{o_{ji}^{\diamondsuit} o_{ji}^{*}}\cap D_j^{\diamondsuit *}.
$$

For $j = 4, i = 1$, X_{41} corresponds to $o_{41}^{\diamondsuit} = 3$ and $o_{41}^{*} = 1$. let us notice that two droplets in the same section can not coalesce since the velocity difference between them is zero. The conservation of mass and momentum are based on

$$
\mathbb{R}_+^2 = \bigcup_{j=1}^{N}\bigcup_{k=1}^{N} L_{jk} = \bigcup_{j=1}^{N}\bigcup_{i=1}^{I^{(j)}}\left(X_{ji}\cup X_{ji}^{\mathrm{sym}}\right)\cup\bigcup_{j=1}^{N} L_{jj},
$$

an equality that can be easily observed in Fig. 1.

References

[1] M. Massot, M. Kumar, A. Gomez, M.D. Smooke, Counterflow spray diffusion flames of heptane: computations and experiments, 27th Symp. on Combustion, The Comb. Institute, 1998, pp. 1975–1983.

[2] J. Hylkema, Modélisation cinétique et simulation numérique d'un brouillard dense de gouttelettes, Application aux propulseurs à poudre, Ph.D. Thesis of ENSAE, 1999.

[3] Y. Tsuji, T. Tanaka, S. Yonemura, Cluster patterns in circulating fluidized beds predicted by numerical simulation (discrete particle versus two-fluid models), Powder Technol. 95 (1998) 254–264.
[4] A. Bracco, P.H. Chavanis, A. Provenzale, A. Spiegel, Particle aggregation in a turbulent Keplerian flow, Phys. Fluids 11 (1999) 2280–2286.
[5] P.H. Chavanis, Trapping of dust by coherent vortices in the solar nebula, Astronom. Astrophys. 356 (2000) 1089–1111.
[6] F.A. Williams, Spray combustion and atomization, Phys. Fluids 1 (1958) 541–545.
[7] F.A. Williams, Combustion theory, in: F.A. Williams (Ed.), Combustion Science and Engineering Series, Addison-Wesley, Reading, MA, 1985.
[8] F. Laurent, M. Massot, Multi-fluid modeling of laminar poly-diperse spray flames: origin, assumptions and comparison of sectional and sampling methods, Combust. Theory Modelling 5 (4) (2001) 537–572.
[9] J.K. Dukowicz, A particle–fluid numerical model for liquid sprays, J. Comput. Phys. 35 (1980) 229–253.
[10] P.J. O'Rourke, Collective drop effects on vaporizing liquid sprays, Ph.D. Thesis, Los Alamos National Laboratory, 87545, 1981.
[11] A.A. Amsden, P.J. O'Rourke, T.D. Butler, KIVA II, A computer program for chemically reactive flows with sprays, Los Alamos National Laboratory Rep. LA-11560-MS, 1989.
[12] P.A. Raviart, L. Sainsaulieu, A nonconservative hyperbolic system modeling spray dynamics. I. Solution of the Riemann problem, Math. Modelling Methods Appl. Sci. 5 (no. 3) (1995) 297–333.
[13] K. Domelevo, L. Sainsaulieu, A numerical method for the computation of the dispersion of a cloud of particles by a turbulent gas flow field, J. Comput. Phys. 133 (no. 2) (1997) 256–278.
[14] M. Rüger, S. Hohmann, M. Sommerfeld, G. Kohnen, Euler/Lagrange calculations of turbulent sprays: the effect of droplet collisions and coalescence, Atomization Sprays 10-1 (2000).
[15] D. Ramkrishna, A.G. Fredrickson, Population Balances: Theory and Applications to Particulate Systems in Engineering, Academic Press, New York, 2000.
[16] D.L. Wright, R. McGraw, D.E. Rosner, Bivariate extension of the quadrature method of moments for modeling simultaneous coagulation and sintering of particle populations, J. Colloid and Interface Sci. 236 (2001) 242–251.
[17] D.L. Marchisio, R.D. Vigil, R.O. Fox, Quadrature method of moments for aggregation-breakage processes, J. Colloid Interface Sci. 258 (2) (2003) 322–334.
[18] D.A. Drew, S.L. Passman, Theory of Multicomponent Fluids, Applied Mathematical Sciences, vol. 135, Springer, New York, 1999.
[19] G. Chanteperdrix, P. Villedieu, J.P. Vila, A compressible model for separated two-phase flows computations, in: ASME FEDSM'02, Paper 31141, ASME Fluids Engineering Division Summer Meeting, Montreal, 2002.
[20] H. Guillard, A. Murrone, A five equation reduced model for compressible two phase flow problems, Prepublication of INRIA 4778, 2003.
[21] J.B. Greenberg, I. Silverman, Y. Tambour, On the origin of spray sectional conservation equations, Combust. Flame 93 (1993) 90–96.
[22] F. Laurent, Modélisation mathématique et numérique de la combustion de brouillards de gouttes polydispersés, Ph.D. Thesis of Université Claude Bernard, Lyon 1, 2002.
[23] M. Massot, Modélisation mathématique des milieux réactifs, Habilitation à Diriger des Recherches Thesis of Université Claude Bernard, Lyon 1, 2003.
[24] F. Laurent, V. Santoro, M. Noskov, M.D. Smooke, A. Gomez, M. Massot, *Accurate treatment of size distribution effects in polydisperse spray diffusion flames: multi-fluid modeling, computations and experiments*, Prepublication of the Laboratory MAPLY 347, 2002, submitted. Available from http://maply.univ-lyon1.fr/publis/publiv/2002/publis.html.
[25] J. Réveillon, M. Massot, C. Péra, Lagrangian/Eulerian analysis of the dispersion of vaporizing polydisperse sprays in turbulent flows, Proceedings of the Summer Program 2002, Center for Turbulence Research, Stanford University, 2002, pp. 393–404.
[26] F. Bouchut, On zero pressure gas dynamics, in: Advances in Kinetic Theory and Computing, World Scientific, River Edge, NJ, 1994., pp. 171–190.
[27] Ya.B. Zeldovich, Gravitational instability: an approximate theory for large density perturbations, Astronom. Astrophys. 5 (1970) 84–89.
[28] F. Laurent, Numerical analysis of a Eulerian multi-fluid method for the description of evaporating sprays, Note aux Comptes Rendus de l'Académie des Sciences de Paris, Série I, Mathématiques, t. 334 (No. 5) (2002) 417–422.
[29] P. Villedieu, J. Hylkema, A random particle method based on a kinetic equation for the numerical simulation of dense sprays of liquid droplets, Note aux Comptes Rendus de l'Académie des Sciences de Paris, Série I, Mathématiques, t. 325 (No. 3) (1997) 323–328.
[30] J. Hylkema, P. Villedieu, A random particle method to simulate coalescence phenomena in dense liquid sprays, Lecture Notes in Physics, vol. 515, Proc. 16th Int. Conf. on Num. Meth. in Fluid Dyn., Arcachon, France, 1998, pp. 488–493.
[31] M. Massot, P. Villedieu, Eulerian multi-fluid modeling for the numerical simulation of polydisperse dense liquid sprays, Note aux Comptes Rendus de l'Académie des Sciences de Paris, Série I, Mathématiques, t. 332 (2001) 869–874.
[32] F. Bouchut, S. Jin, X. Li, Numerical approximations of pressureless and isothermal gas dynamics, SIAM J. Numer. Anal. 41 (1) (2003) 135–158.

[33] B. Abramzon, W.A. Sirignano, Droplet vaporization model for spray combustion calculations, Int. J. Heat Mass Transfer 32 (1989) 1605–1618.
[34] P.R. Brazier-Smith, S.G. Jennings, J. Latham, The interaction falling water drops: coalescence, Proceedings of the Royal Society, London 326 (1972) 393–408.
[35] N. Ashgriz, J.Y. Poo, Coalescence and separation in binary collisions of liquid droplets, Journal of Fluid Mechanics 221 (1990) 183–204.
[36] J. Dupays, Y. Fabignon, P. Villedieu, G. Lavergne, J.L. Estivalezes, Some aspects of two-phase flows in solid propellant rocket motors, in Solid propellant chemistry, combustion and interior balistics, Progress in Astronautics and Aeronautics, Vol 185 (2000).
[37] D.P. Schmidt, C.J. Rudtland, A new droplet collision algorithm, J. Comput. Phys. 164-1 (2000) 62–80.
[38] G.A. Bird, Molecular gas dynamics and the direct simulation of gas flows, Oxford science publications, vol. 42, 1994.
[39] A.C. Hindmarsh, ODEPACK, a systematized collection of ODE solvers, in: R.S. Stepleman et al. (Eds.), Scientific Computing, North-Holland, Amsterdam, 1983.
[40] E. Hairer, G. Wanner, Solving Ordinary Differential Equations II: Stiff and Differential-Algebraic Problems, Springer, New York, 1991.